HHS Public Access

Author manuscript

Gene Expr Patterns. Author manuscript; available in PMC 2020 December 01.

Published in final edited form as:

Gene Expr Patterns. 2019 December ; 34: 119075. doi:10.1016/j.gep.2019.119075.

Sox9 in mouse urogenital sinus epithelium mediates elongation of prostatic buds and expression of genes involved in epithelial cell migration

Andrew J. Schneider[a], **Joseph Gawdzik**[a,c], **Chad M. Vezina**[b,c], **Tracie R. Baker**[c,d], **Richard E. Peterson**[a,c,*]

[a]School of Pharmacy, University of Wisconsin-Madison, 777 Highland Avenue, Madison, WI, 53705, USA

[b]School of Veterinary Medicine, University of Wisconsin-Madison, 1656 Linden Drive, Madison, WI, 53706, USA

[c]Molecular and Environmental Toxicology Center, University of Wisconsin-Madison, 1400 University Avenue, Madison, WI, 53706, USA

[d]Institute of Environmental Health Sciences and School of Medicine, Wayne State University, 6135 Woodward Avenue, Detroit, MI, 48202, USA

Abstract

Previous studies identified *Sox9* as a critical mediator of prostate development but the precise stage when *Sox9* acts had not been determined. A genetic approach was used to delete *Sox9* from mouse urogenital sinus epithelium (UGE) prior to prostate specification. All prostatic bud types (anterior, dorsolateral and ventral) were stunted in *Sox9* conditional knockouts (cKOs) even though the number of prostatic buds did not differ from that of controls. We concluded that *Sox9* is required for prostatic bud elongation and compared control male, control female, *Sox9* cKO male and *Sox9* cKO female UGE transcriptomes to identify potential molecular mediators. We identified 702 sex-dependent and 95 Sox9-dependent genes. Thirty-one genes were expressed in both a sex- and *Sox9*-dependent pattern. A comparison of *Sox9* cKO female vs control female UGE transcriptomes revealed 74 *Sox9*-dependent genes, some of which also function in cell migration. SOX9 regulates, directly or indirectly, a largely different profile of genes in male and female UGE. Eighty-three percent of *Sox9*-dependent genes in male UGE were not *Sox9*-dependent in female UGE. Only 16 genes were *Sox9*-dependent in the UGE of both sexes and seven had cell migration functions. These results support the notion that *Sox9* promotes cell migration activities needed for prostate ductal elongation.

Corresponding author. School of Pharmacy, University of Wisconsin-Madison, 777 Highland Avenue, Madison, WI, 53705, USA. richard.peterson@wisc.edu (R.E. Peterson).

Appendix A. Supplementary data

Supplementary data to this article can be found online at https://doi.org/10.1016/j.gep.2019.119075.

Declaration of competing interest

All authors declare no conflicts of interest.

Data statement

Raw microarray data have been uploaded to the NCBI GEO database. Microarray data are also given in Supplementary Tables 1, 2, 4, 6, 7 and 8.

Keywords

Sox9 conditional knockout; *Sox9*-dependent genes; Sex-dependent genes; Prostate development; Cell migration

1. Introduction

The prostate originates from the urogenital sinus (UGS) in three sequential stages of development (specification, initiation and elongation). Prostate development initiates when fetal androgens bind androgen receptors in UGS mesenchyme (UGM). The activated androgen receptors stimulate release of paracrine signals, including fibroblast growth factors (FGFs), which act on UGS epithelium (UGE) to promote bud formation (Thomson and Cunha, 1999; Prins and Putz, 2008). Prostatic buds are specified across three UGE surfaces: anterior, dorsolateral and ventral. Prostatic buds are initiated as small protrusions extending from the UGE surface (Lin et al., 2003; Vezina et al., 2008). Prostatic buds elongate by invading the UGM, a process that continues postnatally, when buds also undergo extensive branching and canalization to form ductal networks of the anterior, dorsolateral and ventral prostate lobes (Sugimara et al., 1986).

Sry-box 9 (*Sox9*) is involved in a variety of developmental processes (Pritchett et al., 2011) and encodes a transcription factor essential for prostatic bud formation (Huang et al., 2012; Thomsen et al., 2008). Human and mouse prostatic SOX9 expression are predominantly epithelial (Huang et al., 2012; Wang et al., 2008) and are robust in buds during initiation and elongation (Huang et al., 2012; Thomsen et al., 2008; Wang et al., 2008). The best-characterized *Sox9* regulated genes in cartilage and bone are extracellular matrix (ECM) genes, which participate in chondrogenesis (Akiyama, 2008; Oh et al., 2014; Ohba et al., 2015). Outside of cartilage and bone, however, the battery of *Sox9* regulated genes varies between organs (Garside et al., 2015). *Sox9* dependent genes have not until now been identified *in vivo* in the mouse UGE.

The etiology/progression of prostate cancer and benign prostate hyperplasia involve, to some degree, reactivation of signaling pathways, homologous in mouse and human, that direct prostate development (Schaeffer et al., 2008; Schrecengost and Knudsen, 2013; Cunha and Ricke, 2011; Cunha et al., 2018). *Sox9* is essential for mouse prostate development and promotes prostate carcinogenesis in mouse models (Thomsen et al., 2008; 2010; Huang et al., 2012). *Sox9* is expressed during human fetal prostate development and is associated with multiple measures of human prostate cancer (Wang et al., 2008; Schaeffer et al., 2008; Zhong et al., 2012; Qin et al., 2014). Therefore, understanding functional roles of *Sox9* in prostatic bud formation may lead to new strategies or targets for treating prostate cancer and benign prostate hyperplasia.

Two previous studies deleted *Sox9* in the mouse UGS and surprisingly, the outcomes were not the same. Thomsen et al. (2008) used an *Nkx3-1*^{cre} to delete *Sox9* in the UGE and found that ventral prostatic bud formation was inhibited while anterior and dorsolateral bud formation was spared. Huang et al. (2012) used a *ROSA26-ER*^{cre} to delete *Sox9* in UGE and UGM and found that ventral, anterior and dorslolateral bud formation was impaired. While

both studies showed *Sox9* plays a role in prostatic budding, the precise function of *Sox9* remained uncertain.

The present study used a Shh^{cre} driver, deleting *Sox9* from UGE only, to test five major hypotheses. Conditional *Sox9* deletion from mouse UGE, prior to the start of bud formation: (1) disrupts one or more stages (specification, initiation and/or elongation) of bud formation, (2) disrupts formation of one or more prostatic bud types, (3) disrupts expression of *Sox9*-dependent genes in both male and female UGE, (4) disrupts one or more *Sox9*-dependent cellular functions in UGE necessary for bud formation, and (5) identifies genes and cellular functions important for budding by comparing male control and *Sox9* cKO UGE transcriptomes to each other and to female control and *Sox9* cKO UGE transcriptomes.

We found that *Sox9* deletion from the male UGE does not affect bud specification or initiation, but instead impairs bud elongation culminating in “stunted buds”. This phenotype is manifested in all prostatic bud types (anterior, dorsolateral and ventral). We found that *Sox9* dependent genes differ in the male and female UGS and identified candidate genes, including those involved in cell migration, which are likely to mediate *Sox9*-dependent prostatic bud elongation.

2. Results

2.1. SOX9 expression in lower urinary tract and *Sox9* knockout in UGE prior to bud initiation

The lower urinary tract of male mouse fetuses was stained at multiple developmental stages to characterize the temporal expression pattern of SOX9. At E14.5, the earliest stage assessed, no SOX9 expression was observed (Supplementary Fig. 1). By E15.0, SOX9 was detected throughout the epithelium of the bladder, UGS, Wolffian ducts and urethra, and was also detected in mesenchymal cells largely located in close proximity to the UGE (Fig. 1A, left and right panels).

At E18.5, after prostatic buds have initiated and are elongating, SOX9 expression was observed most prominently in the UGE throughout the entire length of prostatic buds (Fig. 1B, left and right panels). This is shown at low magnification for two anterior buds (AB) in a transverse section of the UGS (left) and at high magnification for one of these ABs (right). Careful examination of SOX9 immunostaining in the single AB (right) shows SOX9 is expressed, not only in epithelial cells throughout the bud, but also in some mesenchymal cells in close proximity to the bud surface.

Previous studies have shown that *Sox9* plays an important role in prostate budding/development, but the precise nature of its role is uncertain. To better define its role, we used Shh^{cre} to delete *Sox9* from the UGE and tested the hypothesis that prostatic bud formation *in vivo* requires *Sox9* in the UGE, prior to and during, bud specification, initiation and elongation.

ShhcreERT2/C activity was detected in the entire lower urinary tract epithelium of E9-13 mice (Seifert et al., 2009). This is before prostatic bud formation is initiated. Therefore, we

used a *Shh*$^{cre/+}$ mouse to drive cre expression in UGE at a slightly later stage of development. *Shh*$^{cre/+}$ mice were mated to ROSA26 reporter mice and UGSs from E14.5 fetuses were harvested and stained for β–galactosidase activity using Bluo-gal as the chromogen. Blue staining showed that cre was expressed in bladder and urethral epithelium at E14.5 (Fig. 2A).

To confirm SOX9 was deleted prior to initiation of prostatic budding, UGSs from E16.5 control (*Shh*$^{+/+}$; *Sox9*$^{fl/+}$), and *Sox9* cKO (*Shh*$^{Cre/+}$; *Sox9*$^{fl/fl}$) fetuses (see Table 1) were sectioned and stained by IHC for SOX9. E16.5 is immediately prior to prostatic budding initiation. UGSs from control mice showed SOX9 expression throughout the UGE which tended to increase across the UGE from luminal to mesenchymal surface (Fig. 2B). Some peri-UGE mesenchymal cells of control mice also showed SOX9 expression. By comparison, no SOX9 was observed in lower urinary tract epithelium of *Sox9* cKO mice (Fig. 2C). Importantly, SOX9 expression was seen in Wolffian duct epithelium, peri-UGE mesenchymal cells (arrow), and Sertoli cells in the testis (inset) of *Sox9* cKO mice (Fig. 2C). These internal positive controls establish that *Sox9* deletion was complete and specific to lower urinary tract epithelium.

2.2. Sox9 knockout in male UGE inhibits elongation of all prostatic bud types

IHC staining, using CDH1 antibody to mark the epithelium, was performed on whole UGSs from control and *Sox9* cKO male fetuses and neonates between E18.5 and P0.5 of development after which prostatic buds were counted. Total bud numbers did not differ between control (36.1 ± 3.9, n=9) and *Sox9* cKO (32.3 ± 8.3, n=3) UGSs. The number of anterior buds (ABs, 3.2 ± 0.5 *vs* 3.7 ± 0.3), dorsolateral buds (DLBs, 27.9 ± 3.2 *vs* 26.7 ± 7.8) and ventral buds (VBs, 5.4 ± 0.8 *vs* 2.0 ± 1.2) also did not differ between control and *Sox9* cKO UGSs. We conclude from these results that *Sox9* in UGE is not required for prostatic bud initiation.

We next investigated whether *Sox9* in UGE is required for bud elongation by assessing the length of prostatic buds. *Sox9* cKO prostatic buds were noticeably shorter than controls. More specifically, all bud types (ABs, DLBs and VBs) in 100% of *Sox9* cKO UGSs were shorter than in littermate controls.

Fig. 3 shows representative examples of control (A) and *Sox9* cKO (B) male UGSs from P0.5 littermates. For each UGS, the right panel is an enlargement of the boxed area in the left panel. All bud types in the *Sox9* cKO UGS failed to elongate and this stunted buds phenotype is most easily observed (B, right) for anterior buds (AB, pseudocolored blue) and ventral buds (VB, pseudocolored green). Note one AB in the control UGS (A, right) has already begun to bifurcate/branch.

It is not known if the shorter prostatic buds in *Sox9* cKO UGSs are permanently stunted or if elongation is severely delayed, because *Sox9* cKO fetuses die shortly after birth, likely in part, to impaired lung development (Rockich et al., 2013). However, when comparing lengths of ABs, DLBs and VBs in UGSs from *Sox9* cKO male fetuses at E18.5 to lengths of the same bud types at P0.5 there were no noticeable differences in lengths. This suggests that all prostatic bud types in *Sox9* cKO male fetuses are permanently stunted.

UGSs of control and *Sox9* hets did not differ in bud count (Supplementary Table 10) or visual appearance of bud length. This shows that one copy of *Sox9* is sufficient to promote prostatic bud elongation.

2.3. GO analysis of microarray data from control and *Sox9* cKO male UGE shows cell migration is impaired

To elucidate the molecular mechanism of *Sox9* in the prostatic budding process, total RNA was isolated from UGE of E16.75 control male and *Sox9* cKO male fetuses for microarray analysis. E16.75 was chosen because this is just prior to prostatic bud initiation, when control and *Sox9* cKO male UGSs are still morphologically identical. Compared to control male UGE, 95 annotated transcripts were differentially regulated at least 1.3 fold ($p \leq 0.05$) in male *Sox9* cKO UGE: 63 downregulated and 32 upregulated (Supplementary Table 1). Additionally, 149 (61%) unannotated transcripts were significantly differentially regulated at least 1.3 fold: 71 downregulated and 78 upregulated (Supplementary Table 1).

GO analysis of these differentially regulated, *Sox9*-dependent genes in the male UGE identified 10 pathways or cell functions for which there was significant gene enrichment (Z score < -2.0 or $\geq \pm 2.0$). Eight of the pathways/functions were related to cell migration (Table 2). The Z score for each of the 10 pathways/functions was negative, indicating downregulated or deficient activity.

2.4. Comparison of control male and female UGE transcriptomes

To identify sex-dependent genes that may regulate prostatic bud development, it is essential to compare transcriptomes at E16.75 of control male UGE (which forms prostatic buds) to control female UGE (which does not). This is the same time in development when the *Sox9* cKO male transcriptome was compared to the control male transcriptome to identify *Sox9*-dependent genes in the male UGE.

In this comparison of UGE transcriptomes between sexes, upregulation indicates RNA was more abundant in the male UGE, while downregulation indicates it was less abundant compared to female. In control male UGE, compared to control female UGE, 702 annotated transcripts were significantly differentially regulated ($p \leq 0.05$) at least 1.3 fold: 352 upregulated (RNA more abundant in male) and 350 downregulated (RNA less abundant in male) (Supplementary Table 2). Additionally, 519 (43%) unannotated transcripts were significantly differentially regulated at least 1.3 fold: 221 upregulated and 298 downregulated ($p \leq 0.05$).

2.5. Discovering gene candidates in the UGE for regulating prostatic bud development

To identify UGE candidate genes for the regulation of prostatic bud development, gene expression in the UGE at E16.75 was compared between *Sox9* cKO male (which forms stunted prostatic buds) and control male UGE (which forms elongated buds). This comparison revealed 95 genes that where significantly up or downregulated by *Sox9* cKO in the male UGE (Supplementary Table 1). These genes are referred to as “Male *Sox9*-Dependent”. In addition, since there is a known sex difference in prostatic bud formation (UGE of the control male undergoes extensive bud formation while UGE of the control

female does not) the 702 genes significantly up and downregulated in the male vs female UGE are referred to as “Sex-Dependent” (Supplementary Table 2).

Importantly, among the 95 “Male *Sox9*-Dependent” genes (Supplementary Table 1) and 702 “Sex-Dependent” genes (Supplementary Table 2), only 31 genes have expression that is both “Male *Sox9*-Dependent” and “Sex-Dependent” (union of Venn diagram in Fig. 4). Of these 31, 10 genes have expression in the UGE that is either increased in both a “Male *Sox9*-Dependent” and “Sex-Dependent” manner or decreased in both a “Male *Sox9*-Dependent” and “Sex-Dependent” fashion. Due to this expression pattern, these 10 genes are not considered “candidates” for regulating prostatic bud formation and they are listed in Supplementary Table 3.

On the other hand, the remaining 21 genes are “candidates” for regulating prostatic bud formation and they are given in (Table 3). 18 of these genes may “positively regulate” bud formation. They are: [1] downregulated in *Sox9* cKO male UGE (buds stunted) *vs* control male UGE (buds form) and [2] upregulated in control male UGE (buds form) *vs* control female UGE (buds do not form). These 18 genes include *Sox9*, a known “positive regulator” of bud formation and 17 other “candidate positive regulators” or promoters of prostatic bud formation. In addition, 3 of these genes may “negatively regulate” bud formation. They are: [1] upregulated in *Sox9* cKO male UGE (buds stunted) *vs* control male UGE (buds form) and [2] downregulated in control male UGE (buds form) *vs* control female UGE (buds do not form). These 3 genes are “candidate negative regulators”, genes transcriptionally repressed by *Sox9* that would otherwise inhibit bud formation.

2.6. PCR confirmation of *Sox9* regulated genes in male UGE determined by microarray

Follow-up quantitative PCR, targeting 14 differentially regulated genes in the male UGE determined by microarray (control male *vs Sox9* cKO male; Supplementary Table 1) was carried out using a different RNA pool that was collected from control and *Sox9* cKO UGEs for PCR (Supplementary Table 9). Fig. 5 shows that the PCR results essentially confirmed microarray results. This was the case for genes with various putative functions including: cell migration, prostatic bud promotion, prostatic bud inhibition and other functions. Also for each of the 14 genes assessed by microarray and by PCR in Fig. 5, relative expression levels for “individual UGE samples” are shown as “red dots” in Supplementary Fig. 2 illustrating variance in the data.

2.7. GO analysis of microarray data from control and *Sox9* cKO female UGE also shows cell migration is impaired

Having described the *Sox9* deficient transcriptome of the male UGE (Supplementary Table 1) we did the same for the female UGE (Supplementary Table 4). Total RNA was isolated from UGEs of E16.75 control female and *Sox9* cKO female fetuses for microarray analysis. Compared to the control female UGE, 74 annotated transcripts were differentially regulated at least 1.3 fold in the *Sox9* cKO female UGE: 34 downregulated and 40 upregulated ($p \leq 0.05$). Additionally, 124 (63%) unannotated transcripts were significantly differentially regulated at least 1.3 fold–57 downregulated and 67 upregulated. Gene ontology analysis of the differentially regulated genes in the female UGE identified three pathways or cell

functions for which there was significant gene enrichment (Z score < −2.0 or ≥ +2.0). Two of these were related to cell migration (Supplementary Table 5).

2.8. Comparison of "*Sox9*-Dependent" genes in male and female UGE - notable similarities but marked differences

Comparing the 95 "Male *Sox9*-Dependent" annotated transcripts in the male UGE (Supplementary Table 1) to the 74 "Female *Sox9*-Dependent" annotated transcripts in the female UGE (Supplementary Table 4) revealed 16 annotated transcripts (and 8 unannotated transcripts) that are regulated, in common, by *Sox9* in both sexes (union of Venn diagram in Fig. 6, Table 4 and Supplementary Table 6). Of these 16 genes, 14 were downregulated in the UGE of both sexes and 2 were upregulated. Of the 14 downregulated "*Sox9*-dependent" genes, 7 were shown by GO analysis (*Cdc43ep1, Cxcl14, Cxcr4, Itgb8, Shh, Sox9, Tns4*) to function in cell migration (Table 2; Supplementary Table 5).

The last major finding in comparing "Male *Sox9*-Dependent" to "Female *Sox9*-Dependent" genes in the UGE is that, the majority of these genes were differentially regulated in only the male or female. In the male UGE, 79 (83%) of the 95 "*Sox9*-dependent" genes (Fig. 6) were unique to males whereas in the female UGE, 58 (78%) of 74 such genes (Fig. 6) were unique to females. This sex-dependent difference in the *Sox9* null UGE transcriptome at E16.75 is illustrated by the heatmap in Fig. 7. The highest fold change for the full set of differentially expressed genes, for both genders, was the unannotated transcript identified as TC0500002057.mm.1 in the microarray (5.35 in female and 4.1 in male) (Supplementary Table 7).

3. Discussion

3.1. Major conclusions about the role of *Sox9* in prostate development

We identified *Sox9* protein at an earlier stage of mouse prostate development than previously reported. No expression was observed at E14.5, but by E15.0 SOX9 was expressed in urethra, UGS and bladder epithelium and UGS mesenchyme. We used a Shh^{cre} driver to delete *Sox9* from UGS epithelium prior to onset of budding. In contrast to a previous study describing a regionally restricted role of *Sox9* in ventral prostate development (Thomsen et al., 2008), we show that *Sox9* is required for elongation of all (anterior, dorsolateral and ventral) prostatic buds. *Shhcre;Sox9* knockout mouse prostatic buds appropriately specify and initiate but fail to elongate, resulting in a "stunted buds" phenotype. We performed transcriptomic analysis to reveal possible mechanisms of *Sox9* action. Our results support a model in which *Sox9* functions uniquely in male UGS epithelium to mediate bud outgrowth by potentially enhancing epithelial cell migration.

3.2. A more widely distributed role for *Sox9* in prostatic bud elongation than previously appreciated

Our conclusion that UGS epithelial *Sox9* is required for outgrowth of all mouse prostatic buds differs from two previous reports. Thomsen et al. (2008) used a *Nkx3-1cre;Sox9* knockout to conclude *Sox9* acts regionally to control ventral prostate development without appreciably affecting anterior and dorsolateral prostate development. *Nkx3-1* is first

expressed in the UGS at E15.5 (Keil et al., 2012b) and ventral prostatic buds form after anterior and dorsolateral buds (Lin et al., 2003). A possible reason why ventral prostate development is selectively impaired in *Nkx3-1cre;Sox9* knockouts is that the *cre* is active for a longer period of time in the ventral region, enabling more complete re-combination prior to ventral bud formation. In contrast, complete *Sox9* deletion is attained at least as early as E12.0 in *Shhcre;Sox9* knockout UGS epithelium (Seifert et al., 2009), resulting in widespread defects in prostatic bud elongation. Huang et al. (2012) concluded from the tamoxifen-inducible *Rosa26ERCre-Sox9*$^{flox/flox}$ conditional knockout that *Sox9* is essential for bud initiation and is a mediator of the UGE/prostate epithelial lineage. However, the *cre* driver used in their study is expressed in both UGS epithelium and mesenchyme, differing from the UGS epithelial-specific *Sox9* knockout in our study. Their study was performed *in vitro* while ours was performed *in vivo.* Finally, it is possible that stunted buds developed in the Sox9 mutant UGS organ cultures of Huang et al. (2012), but due to their abnormally small size, were not detected.

3.3. Sox9-dependent transcriptome in UGS epithelium differs from that of other tissues

The *Sox9*-dependent transcriptome in male and female UGEs in the present study revealed few differentially expressed transcripts (< 0.63% of all transcripts) and the fold changes in gene expression that were significant, were modest (1.3 fold cut-off, $p < 0.05$). The developmental stage selected to assess gene expression may play a role. E16.75 is before the start of bud elongation (Lin et al., 2003; Vezina et al., 2008). If we had assessed *Sox9*-dependent gene expression one day later, when far more initiated buds were elongating, fold changes in expression may have been greater. Finally, modest changes in *Sox9*-dependent gene expression are not unique to the UGE. This was also observed in mouse atrioventricular canal and hair follicle stem cell transcriptomes following deletion of *Sox9* (Garside et al., 2015; Kadaja et al., 2014). Thus, *Sox9* functions in the UGS epithelium by modulating the expression of genes as opposed to strongly inducing or repressing their expression.

SOX transcription factors exert their activating or repressive functions on gene expression by binding protein partners (Kamachi and Kondoh, 2013). The combinatorial code of target specificity produced by SOXs and their partner proteins (Soxpartner code) (Kamachi et al., 2000; Kondoh and Kamachi, 2010; Kamachi and Kondoh, 2013) ensures stringent target gene selection. Accordingly, *Sox9*-dependent genes in male UGE differ from those identified in cartilage (Lefebvre et al., 1997; Bridgewater et al., 1998; Sekiya et al., 2000; Xie et al., 1999), chondrocytes (Oh et al., 2014), testes (de Santa Barbara et al., 1998), neural crest (Spokony et al., 2002), intestine (Blache et al., 2004), lung (Rockich et al., 2013), heart (Garside et al., 2015) and, except for *Mia*, conjunctiva (Chen et al., 2014).

3.4. Sox9 function in cell migration fits with Sox9's role in extracellular matrix regulation

Many developing organs require cell migration (Hogan, 1999) including salivary glands (Hauser and Hoffman, 2015; Harunaga et al., 2011), ocular glands (Tsau et al., 2011; Garg and Zhang, 2017), mammary glands (Hinck and Silberstein, 2005), lungs (Weaver et al., 2000; Rockich et al., 2013), kidneys (Chi et al., 2009; Kuure et al., 2010) limbs (Wyngaarden et al., 2010; Hopyan et al., 2011; Hopyan, 2017) and neural crest derived

tissues such as the nervous system (Minoux and Rijli, 2010). *Sox9* is required for cell migration in lung buds (Rockich et al., 2013), in bladder, prostate and lung cancer cells (Ling et al., 2011; Wang et al., 2015; Cai et al., 2013), and in metastatic cell migration in breast, colon, prostate and skin (Chakravarty, et al., 2011; Bowen et al., 2009; Cai et al., 2013; Francis et al., 2018; Wang et al., 2008; Rao et al., 2010).

Our proposed mechanism of *Sox9* as a mediator of epithelial cell migration in prostatic buds is consistent with the established role of *Sox9* in ECM regulation. Migrating cells polarize and then form ECM adhesions before protruding in the direction of migration (Ganser et al., 1991; Hinck and Silberstein, 2005). ECM adhesions act as traction sites for forward movement (Ridley et al., 2003) and ECM components associate with the cell cytoskeleton and influence: cytoskeletal reorganization (Hay, 1982; Nishizaka et al., 2000) and cell migration (Ridley et al., 2003). *Sox9* plays a pivotal role in both (Pritchett et al., 2011).

SOX9 directly binds loci of 18 ECM genes in chondrocytes (Oh et al., 2010) and regulates genes encoding ECM proteins and modifying enzymes (Oh et al., 2014). *Sox9* organizes valvular ECM proteins in heart (Lincoln et al., 2007) and regulates ECM proteins and matrix metalloproteinases (MMPs) in gonads (Georg et al., 2012; Nakamura et al., 2012). *Sox9* mediates fibrotic and sclerotic diseases by promoting excessive and inappropriate ECM deposition (Naitoh et al., 2005; Hanley et al., 2008; Bennett et al., 2007; Sumi et al., 2007; Airik et al., 2010; Schulick et al., 1998). Thus, regulation of the ECM is a critical *Sox9* function.

We identified a subset of *Sox9*-dependent genes in male UGS epithelium (Table 2, Supplementary Table 5) that mediate cell migration. *Cdc42* regulates cell polarity (Ridley et al., 2003) and *Barx2* facilitates cell adhesion and ECM remodeling (Meech et al., 2005; Stevens and Meech, 2006); both crucial for ocular gland bud elongation (Tsau et al., 2011). CXCR4 modulates MMP expression and enhances cell migration (Singh et al., 2004) and *Col14a1* has an adhesive role integrating collagen bundles (Schnittger et al., 1995). Cell migration and ECM remodeling are functions of integrin β8 (Mertens-Walker, et al., 2015) and *Thbsl*, an adhesive glycoprotein, mediates cell-matrix interactions (Hu et al., 2017). *Tns4* binds β integrin, linking ECM to actin cytoskeleton, to promote cell migration (Haynie, 2014). TGFBI, secreted from UGE, interacts with ECM proteins and integrin receptors to decrease cell adhesion (Nummela et al., 2012).

3.5. Putative roles for *Sox9* in UGS epithelial cell migration and distal progenitor cell maintenance

We raise the possibility that prostatic buds fail to elongate in UGE conditional *Sox9* knockouts because of decreases in UGE cell migration, UGE cell proliferation, and/or distal progenitor cell maintenance. Without these potential *Sox9*-dependent functions in the UGS epithelium, we hypothesize that initiated prostatic buds do not elongate, culminating in a “stunted buds” phenotype. This proposed mechanism of action for *Sox9* recognizes that an individual prostatic bud has two parts: proximal base (which attaches to UGS) and distal tip. This distinction is important as cell migration and proliferation during bud elongation are greater distally than proximally (Tsau et al., 2011; Sugimura et al., 1986) and so is SOX9 expression (Wang et al., 2008; Thomsen et al., 2008; Huang et al., 2012). The possibility

that *Sox9* is needed for migration of UGS epithelial cells is predicted by GO analysis of our microarray data collected at E16.75 (Table 2). The notion that *Sox9* is required for proliferation of UGS epithelial cells is suggested by DNA synthesis being reduced in stunted buds of the ventral prostate at E18.5 when *Sox9* is deleted from the UGE (Thomsen et al., 2008). Other studies also show *Sox9* is required for epithelial cell proliferation and migration during bud elongation in the development of other branching organs and for metastasis in cancer (Rockich et al., 2013; Chakravarty, et al., 2011; Bowen et al., 2009; Cai et al., 2013; Francis et al., 2018; Wang et al., 2008; Rao et al., 2010).

4. Experimental Procedures

4.1. Mice, mouse husbandry and tissue collection

All mice were housed in polysulfone cages containing corn cob bedding and maintained on 12 h light/dark cycles at 21 ± 1°C and 20–50% relative humidity. Feed (Harlan Teklad Rodent Diet 8604, Harlan Laboratories Inc., Madison, WI) and water were available *ad libitum.* All procedures were approved by the University of Wisconsin Animal Care and Use Committee and conducted in accordance with the NIH Guide for Care and Use of Laboratory Animals.

The following mice were originally purchased from The Jackson Laboratory (Bar Harbor, ME) and maintained in small breeding colonies in an AAALAC-approved vivarium: C57BL/6J (stock no. 000664), ROSA26 reporter mice (B6.129S4-Gt(ROSA)26Sor^{tm1Sor}/J; Soriano, 1999), mice with a *Shh*$^{cre/+}$ targeted mutation (B6.Cg-Shh$^{tm1(EGFP/cre)Cjt}$/J; Harfe et al., 2004) and mice with a *Sox9*$^{fl/fl}$ targeted mutation (B6.129S7-Sox9^{tm2crm}/J; Akiyama et al., 2002); all genetically engineered mice had a C57BL/6J background.

To obtain timed-pregnant dams, females were paired with males for 2–3 h; the time at which the mating pair was separated was considered embryonic day (E) 0. Pregnant dams were euthanized by CO_2 asphyxiation at different stages of fetal development. Fetuses and neonates (P0.5) were euthanized by decapitation. The entire genitourinary (GU) tract, containing the UGS, was removed from fetuses or neonates and fixed in 10% neutral buffered formalin for approximately 24 h at 4°C. For short-term storage, fixed GU tracts were kept in 70% ethanol at 4°C; for long-term storage, GU tracts went through graded dehydration steps and were kept in 100% ethanol or 100% methanol at −20°C.

4.2. Study design

Table 1 gives the general design, including mating schemes, experimental use and developmental stage of mice in each experimental group.

4.3. β-Galactosidase staining

E14.5 *cre* reporter mouse UGSs were placed in staining buffer (5mM potassium ferricyanide, 2 mM magnesium chloride, 0.01% sodium deoxycholate and 0.02% Nonidet P40 in PBS, pH 7.5). UGS tissues were incubated at 37°C for 5–10 min to equilibrate the UGS to the buffer. Bluo-gal (Gold Biotechnology, B-673–250), a β-galactosidase substrate, was used to stain UGS tissues. Bluo-gal staining solution, 100 mg/ml Bluo-gal dissolved in

N,N-dimethylformamide (Sigma-Aldrich, 227056), was added to a final concentration of 1 mg/ml. UGS tissues were stained for 2 h at 37°C and then fixed with 10% neutral buffered formalin for approximately 24 h at 4°C.

4.4. Immunohistochemistry (IHC)

Control and *Sox9* cKO UGSs were sectioned and immunostained to confirm *Sox9* knockout. Fixed UGS tissues were embedded in paraffin, cut into 5 μm sagittal sections, deparaffinized and rehydrated, treated with 3% hydrogen peroxide for 10 min, boiled in 10 mM sodium citrate for 20 min, and allowed to cool to room temperature to unmask epitopes. Sections were blocked for 2 h with blocking solution: 5% goat serum (Sigma-Aldrich, G9023) and 1% bovine serum albumin (EMD Millipore, 2910) in phosphate buffered saline containing 0.05% Tween-20 (PBST; Sigma-Aldrich, P3563). The Rabbit Anti-SOX9 primary antibody (Abcam ab185230) was diluted 1:250 in blocking solution, applied to the section, and incubated overnight at 4°C. Sections were washed with PBST and subsequently incubated for 1 h with biotinylated goat anti-rabbit IgG secondary antibody (Vector Labs, BA-1000) diluted 1:250 in blocking solution. Sections were washed with PBST and incubated for 30 min with peroxidase-conjugated streptavidin (Vector Labs, PK-6100). After washing with PBST, staining was achieved by incubating sections with ImmPACT DAB solution (Vector Labs, SK-4105) for 2–5 min at room temperature. Sections were counterstained for 20–30 s with Hematoxylin QS (Vector Labs, H-3404) to label nuclei.

4.5. Whole mount (WM) immunohistochemistry (IHC)

Whole mount IHC staining of control, *Sox9* het and *Sox9* cKO UGSs, harvested at E18.5 or P0.5, was done to observe effects of *Sox9* cKO on prostatic budding. Fixed UGSs were rehydrated into PBS and the bladder and urethra were trimmed off. The complete staining procedure was published previously (Keil et al., 2012a). The primary antibody, rabbit anti-mouse CDH1 antibody (Cell Signaling #3195, RRID:AB_2291471), was diluted 1:350 in blocking buffer. The secondary antibody, Horse Anti-rabbit IgG, ImmPRESS VR Reagent (Vector Labs, MP-6401, RRID:AB_2336529), is provided at a ready-to-use concentration. The chromogen used as the enzymatic substrate was ImmPACT DAB (Peroxidase Substrate Kit, Vector, SK-4105).

Stained whole mount UGSs were viewed under a dissecting microscope, and prostatic buds were counted by region – anterior, dorsolateral and ventral – then summed for total bud number. Unpaired Student's t-tests were used to determine if observed differences in bud number between control and *Sox9* cKO male UGSs were significant ($P < 0.05$).

4.6. Separation of UGE from UGS and isolation of RNA from UGE

UGS (with bladder and urethra attached) was harvested from male and female *Sox9* cKO and littermate control fetuses on E16.75. Each UGS was immediately placed into a 1.5 ml microfuge tube containing 300 μl of 1% trypsin (Difco, 215240) in PBS and incubated on ice for 30 min. Collagenase (Sigma, C9891) was added to a final concentration of 1 mg/ml, followed by an additional 30–45 min incubation on ice. A dissecting microscope was used to mechanically separate UGM from UGE, after which the bladder and urethra epithelium were removed, leaving only UGE. Total RNA was purified from each UGE using RNeasy system

(Qiagen, Hilden, Germany) and analyzed using Agilent Bioanalyzer 2100 and Agilent RNA 6000 Pico Kit (Agilent Technologies, Santa Clara, CA, USA).

4.7. RNA isolation, microarray experiments, and data analysis

RNA was isolated from UGE of E16.75 control and *Sox9* cKO male (N = 6 per genotype) and female (N = 5 per genotype) mouse fetuses. RNA quality assessment, labeling, and hybridization to microarray chips was performed at the University of Wisconsin-Madison Biotechnology Gene Expression Center in 2015. At that time, microarray analysis was widely used due to the expense of RNA sequencing. We understand microarray data can have increased false positives, lower detection range, and saturation of high signals compared to RNA-seq technologies. RNA quality was assessed for all 22 samples using an Agilent 2100 Bioanalyzer. The RNA Integrity Number (RIN) was ≥5.5 for each RNA sample, and the average RIN for all 22 RNAs was 7.3. 2ng of total RNA per sample was amplified and labeled using GeneChip WT Pico Reagent Kit (Affymetrix, Santa Clara, CA, USA), then hybridized to GeneChip Mouse Gene 1.0 ST Array (Affymetrix, Santa Clara, CA, USA) according to manufacturer's protocol.

Microarray data were analyzed using Transcriptome Analysis Console (TAC; Affymetrix, Santa Clara, CA, USA). A transcript was considered differentially regulated (compared to a control) if it had an absolute fold change in abundance of ≥1.3 and $p \leq 0.05$. Due to the low number of annotated differentially expressed genes, we used this cut-off as a broad screening tool for potential targets of interest. Also, due to tissue heterogeneity, low fold changes can have biological relevance which we wanted to capture. The stringency criteria of considering false positive rates of differentially expressed genes ($p<0.05$) as the minimum fold change to be significant was determined based on microarray validation and assessment described previously (Nobis et al., 2003; Huggins et al., 2008; Bigler et al., 2013, Laurent et al., 2013). An annotated transcript was defined as one having a gene symbol or description following TAC analysis; if these were absent the transcript was considered unannotated. Annotated transcripts from the "Male *Sox9*-Dependent" (control male vs *Sox9* cKO male), or "Female *Sox9*-Dependent" (control female vs *Sox9* cKO female) comparisons were entered into Ingenuity Pathway Analysis software (IPA; Qiagen, Hilden, Germany) for further analysis. This included gene ontology (GO) analysis for which an IPA-generated z score of ≤ -2.0 or ≥ 2.0 was considered significant ($p \leq 0.05$). Lists of all differentially expressed genes including for each gene: bi-weight average signal (log2), standard deviation, fold change (linear), ANOVA p-value and FDR-adjusted p-value (q-value), are provided in Supplementary Tables 1, 2 and 4, respectively. All raw microarray data (significant and nonsignificant) from each one of the individual UGE samples used in the present study were uploaded, separately, to the NCBI GEO database (GSE113011; reviewer token mhizgciwxxcxbyl).

4.8. Heatmap construction

Microarray data were extracted from Supplementary Table 1 (*Sox9* cKO male *vs* control male) and Supplementary Table 4 (*Sox9* cKO female *vs* control female). The fold change, gene symbol, description, and grouping was extracted and merged together in Supplementary Table 7. This file was then filtered to remove any unknown gene symbols

and saved as Supplementary Table 8. A heatmap was generated with the fold change and clustered using Euclidean distance (Fig. 7) from the data in Supplementary Table 8. All data processing and visualization was done using R and gplots.

4.9. Quantitative real-time polymerase chain reaction (qRT-PCR)

All UGE tissues used for qRT-PCR were separate and distinct from those used for microarray analysis and were used to confirm microarray results. For qRT-PCR, as done previously for microarray, UGEs isolated from male, *Sox9* cKO and littermate control fetuses on E16.75 were homogenized and total RNA purified using RNeasy (Qiagen, Hilden, Germany). Individual genes assessed by qRT-PCR were selected from those differentially expressed genes identified earlier by microarray (Supplementary Table 1). RNA from the UGE samples designated for qRT-PCR were then used to validate 14 genes of interest as being differentially expressed between, *Sox9* cKO and littermate control male UGEs on E16.75 using Taqman Gene Expression Assays (Life Technologies) and Applied Biosystems 7900 analysis.

More specifically, 10 μl of RNA (4.1 ng/μl) was reverse transcribed with random hexamers and Multiscribe MuLv from the High Capacity cDNA Reverse Transcription Kit (ThermoFisher Scientific) per manufacturer's protocol. 10 μl of resulting cDNA was preamplified for genes selected through microarray analysis or other genes of interest using TaqMan Preamp Mastermix Kit (ThermoFisher Scientific) for 40 cycles in a 50 μl reaction volume. Probes used were Taqman gene expression assays (ThermoFisher Scientific) for *Tns4* (Mm00553421_m1), *Adamts9* (Mm00614433_m1), Plod2 (Mm00478767_m1), *Col14a1* (Mm00805269_m1), *Thbsl* (Mm00449032_g1), *Mia* (Mm00444563_m1), *Sbspon* (Mm01237899_m1), *Cxcr4* (Mm01996749_s1), *Bmp3* (Mm00557790_m1), *Hr* (Mm00498963_m1), *Cxcl14* (Mm00444699_m1), *Shh* (Mm00436528_m1), *Epas1* (Mm01236112_m1), *Sox9* (Mm00448840_m1), *Actb1* (Mm02619580_g1) and *Gapdh* (Mm99999915_g1). Probes were chosen based on best coverage according to ThermoFisher database. Taqman gene expression assays are MIQE compliant and qRT-PCR was performed following MIQE. qRT-PCR reactions for the above genes were performed with Taqman Universal Master Mix (ThermoFisher Scientific) in a 20 μl reaction volume containing 2 μl of the preamplified cDNA. Thermal cycling parameters were carried out per manufacturer's protocol. Reactions were done in triplicate. qRT-PCR analysis and calculations were performed in the Sequence Detection System v 2.4. All transcripts examined were normalized to *Actbl* through the comparative C_t (ΔΔ Ct) method (Livak and Schmittgen, 2001). *Actb1* was unaltered by *Sox9* cKO in both the microarray and qRT-PCR, and thus was suitable as the housekeeping gene. Differences in gene expression between *Sox9* cKO and control UGEs of male and female fetuses, respectively, were determined by comparing the expression values for each gene relative to *Actb1*. Relative expression = $2^{-(\mathrm{Ct}\ goi\ -\ \mathrm{Ct}\ Actb1)} = 2^{-\Delta\mathrm{Ct}}$ where Ct means threshold cycle, and *goi* and *Actbl* refer to gene of interest and beta actin. A one-tailed Student's t-test was then used to identify significant differences between the relative expression of each analyzed gene ($p \leq 0.05$) between male *Sox9* cKO (n=4) and control (n=4) UGEs. The fold change in expression ($2^{-\Delta\Delta\mathrm{Ct}}$) for each gene with respect to the *Sox9* cKO condition was calculated by dividing the mean relative

expression value of the *Sox9* cKO UGEs by the mean relative expression value of the control UGEs (Supplementary Table 9).

Supplementary Material

Refer to Web version on PubMed Central for supplementary material.

Acknowledgments

The authors thank the University of Wisconsin-Madison, Biotechnology Gene Expression Center for providing Affymetrix GeneChip services. The authors also thank Dr. Chris Bradfield, University of Wisconsin-Madison, for advice on experimental design of microarray experiments, Drs. Robert Tanguay and Lisa Truong, Oregon State University, for assistance with heatmap construction of *Sox9*-dependent gene expression results for male and female UGEs in microarray experiments, and Dr. Bridget Baker for manuscript editing suggestions.

Funding

This research was supported by NIH grant ES001332 to REP and CMV, American Foundation for Pharmaceutical Education (AFPE) fellowship to JG and University of Wisconsin-Madison, Molecular and Environmental Toxicology Center, NIH Training Grant (T32-ES007015) to JG. Funding was provided to TRB by the National Center for Advancement of Translational Sciences (K01 OD010462) and Wayne State University Center for Urban Responses to Environmental Stressors (P30 ES020957).

Abbreviations

A	anterior
AB	anterior bud
Array	microarray
BL	bladder
CDH1	Cadherin-1
cKO	conditional knockout
Con	control
Cre	creates re-combination
Cxcr4	C-X-C motif chemokine receptor 4
D	dorsal
DB	dorsal bud
DHT	5α-dihydrotestosterone
DLB	dorsolateral bud
E	embryonic day
ECM	extracellular matrix
ER	estrogen receptor

FGF	fibroblast growth factor
GO	gene ontology
GU	genitourinary
het	heterozygous
IHC	immunohistochemistry
IPA	ingenuity pathway analyses
Mia	melanoma inhibitory activity
MIAME	minimal information about a microarray experiment
MIQE	minimum information for the publication of qPCR experiments
MMP	matrix metalloproteinase
ns	no significant difference
P	postnatal day
PBST	phosphate buffered saline containing 0.05% Tween-20
SV	seminal vesicle
Shh	sonic hedgehog
qRT-PCR	quantitative real-time polymerase chain reaction
Sox9	sry-box 9
TAC	Transcriptome Analysis Console
UGS	urogenital sinus
UGE	urogenital sinus epithelium
UGM	urogenital sinus mesenchyme
UR	urethra
V	ventral
VB	ventral bud
WD	wolffian duct
WM	whole mount

References

Airik R, Trowe MO, Foik A, Farin HF, Petry M, Schuster-Gossler K, Schweizer M, Scherer G, Kist R, Kispert A, 2010 Hydroureternephrosis due to loss of Sox9-regulated smooth muscle cell differentiation of the ureteric mesenchyme. Hum. Mol. Genet 19, 4918–4929. [PubMed: 20881014]

Akiyama H, 2008 Control of chondrogenesis by the transcription factor Sox9. Mod. Rheumatol 18, 213–219. [PubMed: 18351289]

Akiyama H, Chaboissier MC, Martin JF, Schedl A, De Crombrugghe B, 2002 The transcription factor Sox9 has essential roles in successive steps of the chondrocyte differentiation pathway and is required for expression of Sox5 and Sox6. Genes Dev. 16, 2813–2828. [PubMed: 12414734]

Bennett MR, Czech KA, Arend LJ, Witte DP, Devarajan P, Potter SS, 2007 Laser capture microdissection-microarray analysis of focal segmental glomerulosclerosis glomeruli. Nephron 107, e30–e40. [PubMed: 17684420]

Bigler J, Rand HA, Kerkof K, Timour M, Russell CB, 2013 Cross-study homogeneity of psoriasis gene expression in skin across a large expression range. PLoS One. 8, e52242. [PubMed: 23308107]

Blache P, van de Wetering PM, Duluc I, Domon C, Berta P, Freund J-N, Clevers H, Jay P, 2004 SOX9 is an intestine crypt transcription factor, is regulated by the Wnt pathway, and represses the *CDX2* and *MUC2* genes. J. Cell Biol 166, 37–47. [PubMed: 15240568]

Bowen KA, Doan HQ, Zhou BP, Wang Q, Zhou Y, Rychahou PG, Evers BM, 2009 PTEN loss induces epithelial-mesenchymal transition in human colon cancer cells. Anticancer Res. 29, 4439–4449. [PubMed: 20032390]

Bridgewater LC, Lefebvre V, de Crombrugghe B, 1998 Chondrocyte-specific enhancer elements in the Col11a2 gene resemble the Col2a1 tissue-specific enhancer. J. Biol. Chem 273, 14998–15006. [PubMed: 9614107]

Cai C, Wang H, He HH, Chen S, He L, Ma F, Mucci L, Wang Q, Fiore C, Sowalsky AG, Loda M Liu XS, Brown M, Balk SP, Yuan X, 2013 ERG induces androgen receptor-mediated regulation of SOX9 in prostate cancer. J. Clin. Invest 123, 1109–1122. [PubMed: 23426182]

Chakravarty G, Moroz K, Makridakis NM, Lloyd SA, Galvez SE, Canavello PR, Lacey MR, Agrawal K, Mondal D, 2011 Prognostic significance of cytoplasmic SOX9 in invasive ductal carcinoma and metastatic breast cancer. Exp. Biol. Med 236, 145–155.

Chen Z, Huang J, Liu Y, Dattilo LK, Huh S-H, Ornitz D, and Beebe DC, 2014 FGF signaling activates a Sox9-Sox10 pathway for the formation and branching morphogenesis of mouse ocular glands. Development 141, 2691–2701. [PubMed: 24924191]

Chi X, Michos O, Shakya R, Riccio P, Enomoto H, Licht JD, Asai N, Takahashi M, Ohgami N, Kato M, Mendelsohn C, Costantini F, 2009 Ret-dependent cell rearrangements in the Wolffian duct epithelium initiate ureteric bud morphogenesis Dev. Cell 17, 199–209.

Cunha GR, Ricke WA, 2011 A historical perspective on the role of stroma in the pathogenesis of benign prostatic hyperplasia. Differentiation 82, 168–172. [PubMed: 21723032]

Cunha GR, Vezina CM, Isaacson D, Ricke WA, Timms BG, Cao M, Franco O, Baskin LS, 2018 Development of the human prostate. Differentiation 103, 24–45. [PubMed: 30224091]

de Santa Barbara P, Bonneaud N, Boizet B, Desclozeaux M, Moniot B, Sudbeck P, Scherer G, Poulat F, Berta P, 1998 Direct interaction of SRY-related protein Sox9 and steroidogenic factor 1 regulates transcription of the human anti-mullerian hormone gene. Mol. Cell. Biol 18, 6653–6665. [PubMed: 9774680]

Francis JC, Capper A, Ning J, Knight E, de Bono J, Swain A, 2018 SOX9 is a driver of aggressive prostate cancer by promoting invasion, cell fate and cytoskeleton alterations and epithelial to mesenchymal transition. Oncotarget 9, 7604–7615. [PubMed: 29484136]

Ganser GL, Stricklin GP, Matrisian LM, 1991 EGF and TGF alpha influence in vitro lung development by the induction of matrix-degrading metalloproteinases. Int. J. Dev. Biol 35, 453–461. [PubMed: 1801870]

Garg A, Zhang X, 2017 Lacrimal gland development: from signaling interactions to regenerative medicine. Dev. Dyn 246, 970–980. [PubMed: 28710815]

Garside VC, Cullum R, Alder O, Lu DY, Vander Werff R, Bilenky M, Zhao Y, Jones SJ, Marra MA, Underhill TM, Hoodless PA, 2015 SOX9 modulates the expression of key transcription factors required for heart valve development. Development 142, 4340–4350. [PubMed: 26525672]

Georg I, Barrionuevo F, Wiech T, Scherer G, 2012 Sox9 and Sox8 are required for basal lamina integrity of testis cords and for suppression of FOXL2 during embryonic testis development in mice. Biol. Reprod 87, 1–11.

Hanley KP, Oakley F, Sugden S, Wilson DI, Mann DA, Hanley NA 2008 Ectopic SOX9 mediates extracellular matrix deposition characteristic of organ fibrosis. J. Biol. Chem 283, 14063–14071. [PubMed: 18296708]

Harfe BD, Scherz PJ, Nissim S, Tian H, McMahon AP, Tabin CJ, 2004 Evidence for an expansion-based temporal Shh gradient in specifying vertebrate digit identities. Cell 118, 517–528. [PubMed: 15315763]

Harunaga J, Hsu JC, Yamada KM, 2011 Dynamics of salivary gland morphogenesis. J. Dent. Res 90, 1070–1077. [PubMed: 21487116]

Hauser BR, Hoffman MP, 2015 Regulatory mechanisms driving salivary gland organogenesis. Curr. Top. Dev. Biol 115, 111–130. [PubMed: 26589923]

Hay ED, 1982 Interaction of embryonic surface and cytoskeleton with extracellular matrix. Am. J. Anat 165, 1–12. [PubMed: 7137055]

Haynie DT, 2014 Molecular physiology of the tensin brotherhood of integrin adaptor proteins. Proteins 82, 1113–1127. [PubMed: 24634006]

Hinck L, Silberstein GB, 2005 The mammary end bud as a motile organ. Breast Cancer Res. 7, 245–251. [PubMed: 16280048]

Hogan BL, 1999 Morphogenesis. Cell 96, 225–233. [PubMed: 9988217]

Hopyan S, 2017 Biophysical regulation of early limb bud morphogenesis. Dev. Biol 429, 429–433. [PubMed: 28669818]

Hopyan S, Sharpe J, Yan Y, 2011 Budding behaviors: Growth of the limb as a model of morphogenesis. Dev. Dyn 240, 1054–1062. [PubMed: 21384474]

Hu C, Wen J, Gong L, Chen X, Wang J, Hu F, Zhou Q, Liang J, Wei L, Shen Y, Zhang W, 2017 Thrombospondin-1 promotes cell migration, invasion and lung metastasis of osteosarcoma through FAK dependent pathway. Oncotarget 8, 75881–75892. [PubMed: 29100277]

Huang Z, Hurley PJ, Simons BW, Marchionni L, Berman DM, Ross AE, Schaeffer EM, 2012 Sox9 is required for prostate development and prostate cancer initiation. Oncotarget 3, 651–663. [PubMed: 22761195]

Huggins CE, Domenighetti AA, Ritchie ME, Khalil N, Favaloro JM, Proietto J, Smyth GK, Pepe S, Delbridge LM, 2008 Functional and metabolic remodeling in GLUT4-deficient hearts confers hyper-responsiveness to substrate intervention. J. Mol. Cell. Cardiol 44, 270–80. [PubMed: 18191142]

Kadaja M, Keyes BE, Lin M, Pasolli HA, Genander M, Polak L, Stokes N, Zheng D, Fuchs E, 2014 SOX9: A stem cell transcriptional regulator of secreted niche signaling factors. Genes Dev. 28, 328–341. [PubMed: 24532713]

Kamachi Y, Kondoh H, 2013 Sox proteins: regulators of cell fate specification and differentiation. Development 140, 4129–4144. [PubMed: 24086078]

Kamachi Y, Uchikawa M, Kondoh H, 2000 Pairing SOX off: with partners in the regulation of embryonic development. Trends Genet. 16, 182–187. [PubMed: 10729834]

Keil KP, Mehta V, Abler LL, Joshi PS, Schmitz CT, Vezina CM, 2012a Visualization and quantification of mouse prostate development by in situ hybridization. Differentiation 84, 232–239. [PubMed: 22898663]

Keil KP, Mehta V, Branam AM, Abler LL, Buresh-Stiemke RA, Joshi PS, Schmitz CT, Marker PC, Vezina CM, 2012b Wnt inhibitory factor 1 (Wif1) is regulated by androgens and enhances androgen-dependent prostate development. Endocrinology 153, 6091–6103. [PubMed: 23087175]

Kondoh H, Kamachi Y, 2010 SOX-partner code for cell specification: Regulatory target selection and underlying molecular mechanisms. Int. J. Biochem. Cell Biol 42, 391–399. [PubMed: 19747562]

Kuure S, Cebrian C, Machingo Q, Lu BC, Chi X, Hyink D, D'Agati V, Gurniak C, Witke W, Costantini F, 2010 Actin depolymerizing factors Cofilin1 and Destrin are required for ureteric bud branching morphogenesis. PLoS Genet. 6, e1001176. [PubMed: 21060807]

Laurent GS, Shtokalo D, Tackett MR, Yang Z, Vyatkin Y, Milos PM, Seilheimer B, McCaffrey TA, Kapranov P, 2013 On the importance of small changes in RNA expression. Methods 63, 18–24. [PubMed: 23563143]

Lefebvre V, Huang W, Harley VR, Goodfellow PN, de Crombrugghe B 1997 SOX9 is a potent activator of the chondrocyte-specific enhancer of the proa1 (II) collagen gene. Mol. Cell. Biol 17, 2336–2346. [PubMed: 9121483]

Lin T-M, Rasmussen NT, Moore RW, Albrecht RM, Peterson RE, 2003 Region-specific inhibition of prostatic epithelial bud formation in the urogenital sinus of C57BL/6 mice exposed in utero to 2,3,7,8-tetrachlorodibenzo-p-dioxin. Toxicol. Sci 76, 171–181. [PubMed: 12944588]

Lincoln J, Kist R, Scherer G, Yutzey KE, 2007 Sox9 is required for precursor cell expansion and extracellular matrix organization during mouse heart valve development. Dev. Biol 305, 120–132. [PubMed: 17350610]

Ling S, Chang X, Schultz L, Lee TK, Chaux A, Marchionni L, Netto GJ, Sidransky D, Berman DM, 2011 An EGFR-ERK-SOX9 signaling cascade links urothelial development and regeneration to cancer. Cancer Res. 71, 3812–3821. [PubMed: 21512138]

Livak KJ, Schmittgen TS, 2001 Analysis of relative gene expression data using real-time quantitative PCR and the 2(-delta delta C(T)) method. Methods 25, 402–408. [PubMed: 11846609]

Meech R, Edelman DB, Jones FS, Makarenkova HP, 2005 The homeobox transcription factor Barx2 regulates chondrogenesis during limb development. Development 132, 2135–2146. [PubMed: 15800003]

Mertens-Walker I, Fernandini BC, Maharaj MSN, Rockstroh A, Nelson CC, Herington AC, Stephenson S-A, 2015 The tumour-promoting receptor tyrosine kinase, EphB4, regulates expression of Integrin-p8 in prostate cancer cells. BMC Cancer 15, 164. [PubMed: 25886373]

Minoux M, Rijli FM, 2010 Molecular mechanisms of cranial neural crest cell migration and patterning in craniofacial development. Development 137, 2605–2621. [PubMed: 20663816]

Naitoh M, Kubota H, Ikeda M, Tanaka T, Shirane H, Suzuki S, Nagata K, 2005 Gene expression in human keloids is altered from dermal to chondrocytic and osteogenic lineage. Genes Cells 10, 1081–1091. [PubMed: 16236136]

Nakamura S, Watakabe I, Nishimura T, Toyoda A, Taniguchi Y, Tanaka M, 2012 Analysis of medaka sox9 orthologue reveals a conserved role in germ cell maintenance. PLoS ONE 7, e29982. [PubMed: 22253846]

Nishizaka T, Shi Q, Sheetz MP 2000 Position-dependent linkages of fibronectin-integrin-cytoskeleton. Proc. Natl. Acad. Sci. U.S.A 97, 692–697. [PubMed: 10639141]

Nobis W, Ren X, Suchyta SP, Suchyta TR, Zanella AJ, Coussens PM, 2003 Development of a porcine brain cDNA library, EST database, and microarray resource. Physiol. Genomics 16, 153–159. [PubMed: 14559975]

Nummela P, Lammi J, Soikkeli J, Saksela O, Laakkonen P, Hölttä E, 2012 Transforming growth factor beta-induced (TGFBI) is an anti-adhesive protein regulating the invasive growth of melanoma cells. Amer. J. Pathol 180, 1663–1674. [PubMed: 22326753]

Oh CD, Lu Y, Liang S, Mori-Akiyama Y, Chen D, de Crombrugghe B, Yasuda H, 2014 SOX9 regulates multiple genes in chondrocytes, including genes encoding ECM proteins, ECM modification enzymes, receptors, and transporters. PLOS ONE 9, 1–10.

Oh C-D, Maity SN, Lu J-F, Zhang J, Liang S, Coustry F, de Crombrugghe B, Yasuda H, 2010 Identification of SOX9 interaction sites in the genome of chondrocytes. PLOS ONE 5, e10113. [PubMed: 20404928]

Ohba S, He X, Hojo H, McMahon AP, 2015 Distinct transcriptional programs underlie Sox9 regulation of the mammalian chondrocyte. Cell Rep. 12, 229–243. [PubMed: 26146088]

Prins GS, Putz O, 2008 Molecular signaling pathways that regulate prostate gland development. Differentiation 76, 641–659. [PubMed: 18462433]

Pritchett J, Athwal V, Roberts N, Hanley NA, Hanley KP, 2011 Understanding the role of SOX9 in acquired diseases: Lessons from development. Trends Mol. Med 17, 166–174. [PubMed: 21237710]

Qin GQ, He HC, Han ZD, Liang YX, Yang SB, Huang YQ, Zhou L, Fu H, Li JX, Jiang FN, Zhong WD, 2014 Combined overexpression of HIVEP3 and SOX9 predicts unfavorable biochemical recurrence-free survival in patients with prostate cancer. Oncotargets Ther. 7, 137–146.

Rao P, Fuller GN, Prieto VG, 2010 Expression of Sox-9 in metastatic melanoma - a potential diagnostic pitfall. Am. J. Dermatopathol 32, 262–266. [PubMed: 20098296]

Ridley AJ, Schwartz MA, Burridge K, Firtel RA, Ginsberg MH, Borisy G, Parsons JT, Horwitz AR, 2003 Cell migration: Integrating signals from front to back. Science 302, 1704–1709. [PubMed: 14657486]

Rockich BE, Hrycaj SM, Shih HP, Nagy MS, Ferguson MA, Kopp JL, Sander M, Wellik DM, Spence JR, 2013 Sox9 plays multiple roles in the lung epithelium during branching morphogenesis. Proc. Natl. Acad. Sci. U.S.A 110, 4456–4464.

Schaeffer EM, Marchionni L, Huang Z, Simons B, Blackman A, Yu W, Parmigiani G, Berman DM, 2008 Androgen-induced programs for prostate epithelial growth and invasion arise in embryogenesis and are reactivated in cancer. Oncogene 27, 7180–7191. [PubMed: 18794802]

Schnittger S, Herbst H, Schuppan D, Dannenberg C, Bauer M, Fonatsch C, 1995 Localization of the undulin gene (UND) to human chromosome band 8q23. Cytogenet. Cell Genet 68, 233–234. [PubMed: 7842743]

Schrecengost R, Knudsen KE, 2013 Molecular pathogenesis and progression of prostate cancer. Semin. Oncol 40, 244–258. [PubMed: 23806491]

Schulick AH, Taylor AJ, Zuo W, Qiu C, Dong G, Woodward RN, Agah R, Roberts AB, Virmani R, Dichek DA, 1998 Overexpression of transforming growth factor β1 in arterial endothelium causes hyperplasia, apoptosis, and cartilaginous metaplasia. Proc. Natl. Acad. Sci. U.S.A 95, 6983–6988. [PubMed: 9618525]

Seifert AW, Bouldin CM, Choi K-Y, Harfe BD, Cohn MJ, 2009 Multiphasic and tissue-specific roles of sonic hedgehog in cloacal septation and external genitalia development. Development 136, 3949–3957. [PubMed: 19906862]

Sekiya I, Tsuji K, Koopman P, Watanabe H, Yamada Y, Shinomiya K, Nifuji A, Noda M, 2000 SOX9 enhances aggrecan gene promoter/enhancer activity and is up-regulated by retinoic acid in a cartilage-derived cell line, TC6. J. Biol. Chem 275, 10738–10744. [PubMed: 10753864]

Singh S, Singh UP, Grizzle WE, Lillard JW Jr., 2004 CXCL12-CXCR4 interactions modulate prostate cancer cell migration, metalloproteinase expression and invasion. Lab. Invest 84, 1666–1676. [PubMed: 15467730]

Soriano P, 1999 Generalized lacZ expression with the ROSA26 Cre reporter strain. Nat. Genet 21, 70–71. [PubMed: 9916792]

Spokony RF, Aoki Y, Saint-Germain N, Magner-Fink E, Saint-Jeannet JP, 2002 The transcription factor Sox9 is required for cranial neural crest development in Xenopus. Development 129, 421–432. [PubMed: 11807034]

Stevens TA and Meech R 2006 BARX2 and estrogen receptor-alpha (ESR1) coordinately regulate the production of alternatively spliced ESR1 isoforms and control breast cancer cell growth and invasion. Oncogene 25, 5426–5435. [PubMed: 16636675]

Sugimura Y, Cunha GR, Donjacour AA, 1986 Morphogenesis of ductal networks in the mouse prostate. Biol. Reprod 34, 961–971. [PubMed: 3730488]

Sumi E, Iehara N, Akiyama H, Matsubara T, Mima A, Kanamori H, Fukatsu A, Salant DJ, Kita T, Arai H, Doi T, 2007 SRY-related HMG box 9 regulates the expression of Col4a2 through transactivating its enhancer element in mesangial cells. Am. J. Pathol 170, 1854–1864. [PubMed: 17525254]

Thomsen MK, Ambroisine L, Wynn S, Cheah KSE, Foster CS, Fisher G, Berney DM, Møller H, Reuter VE, Scardino P, Cuzick J, Ragavan N, Singh PB, Martin FL, Butler CM, Cooper CS, Swain A, 2010 SOX9 elevation in the prostate promotes proliferation and cooperates with PTEN loss to drive tumor formation. Cancer Res. 70, 979–987. [PubMed: 20103652]

Thomsen MK, Butler CM, Shen MM, Swain A, 2008 Sox9 is required for prostate development. Dev. Biol 316, 302–311. [PubMed: 18325490]

Thomson AA, Cunha GR, 1999 Prostatic growth and development are regulated by FGF10. Development 126, 3693–3701. [PubMed: 10409514]

Tsau C, Ito M, Gromova A, Hoffman MP, Meech R, Makarenkova HP, 2011 Barx2 and Fgf10 regulate ocular glands branching morphogenesis by controlling extracellular matrix remodeling. Development 138, 3307–3317. [PubMed: 21750040]

Vezina CM, Allgeier SH, Moore RW, Lin T-M, Bemis JC, Gasiewicz TA, Peterson RE, 2008 Dioxin causes ventral prostate agenesis by disrupting dorsoventral patterning in developing mouse prostate. Toxicol. Sci 106, 488–496. [PubMed: 18779384]

Wang H, Leav I, Ibaragi S, Wegner M, Guo-fu H, Lu ML, Balk SP, Yuan X, 2008 SOX9 is expressed in human fetal prostate epithelium and enhances prostate cancer invasion. Cancer Res. 68, 1625–1630. [PubMed: 18339840]

Wang X, Ju Y, Zhou M, Liu X, Zhou C, 2015 Upregulation of SOX9 promotes cell proliferation, migration and invasion in lung adenocarcinoma. Oncol. Lett 10, 990–994. [PubMed: 26622611]

Weaver M, Dunn NR, Hogan BLM, 2000 Bmp4 and Fgf10 play opposing roles during lung bud morphogenesis. Development 127, 2695–2704. [PubMed: 10821767]

Wyngaarden LA, Vogeli KM, Ciruna BG, Wells M, Hadjantonakis AK, Hopyan S, 2010 Oriented cell motility and division underlie early limb bud morphogenesis. Development 137, 2551–2558. [PubMed: 20554720]

Xie WF, Zhang X, Sakano S, Lefebvre V, Sandell LJ, 1999 Trans-activation of the mouse cartilage-derived retinoic acid-sensitive protein gene by Sox9. J. Bone Miner. Res 14, 757–63. [PubMed: 10320524]

Zhong W.-d., Qin G.-q., Dai Q.-s., Han Z.-d., Chen S.-m., Ling X.-h., Xin F, Chao C, Chen J.-h., Chen X.-b., Lin Z.-y., Deng Y.-h., Wu S.-l., He H.-c., Wu C.-l., 2012 SOXs in human prostate cancer: Implication as progression and prognosis factors. BMC Cancer 12, 248. [PubMed: 22703285]

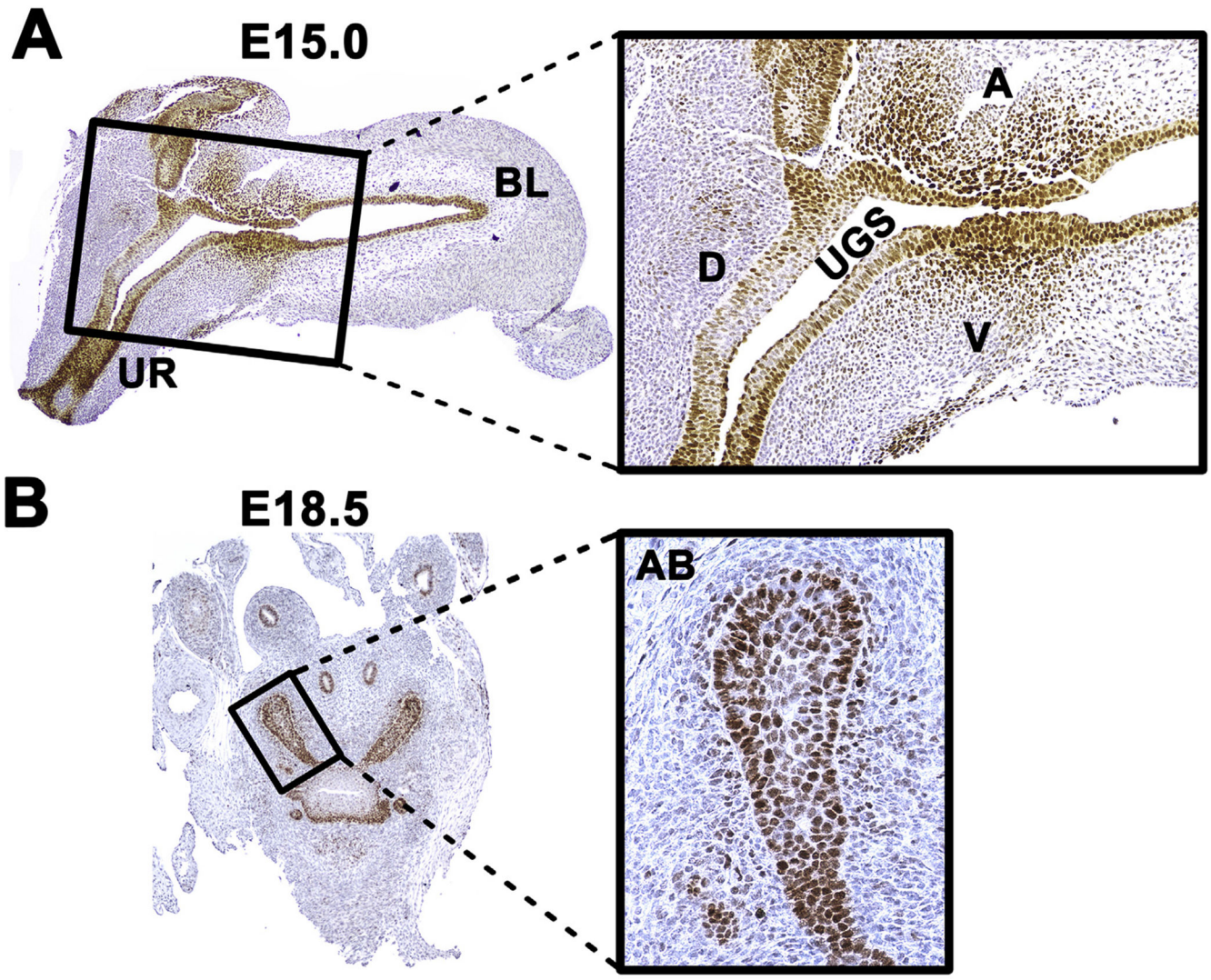

Fig. 1.

Expression of SOX9 in lower urogenital tract and prostatic buds of the male mouse fetus. (A, left panel) IHC showing SOX9 expression in a sagittal section of the lower urogenital tract at E15.0. Brown staining is seen throughout epithelium of the bladder (BL), Wolffian ducts (WD), UGS and urethra (UR), and in patches of UGS mesenchyme [40x]. (A, right panel) SOX9 expression in the UGS is visualized at higher magnification [100x]. (B, left panel) SOX9 expression is shown for two anterior buds in a transverse section of UGS at E18.5 [40x] and (B, right panel) in a single anterior bud (AB) at E18.5 [200x]. Nuclei were counterstained blue with hematoxylin. Other abbreviations: anterior (A), dorsal (D) and ventral (V) regions of the UGS. Images are representative of n=3 litter independent fetuses, where each fetus came from a different litter.

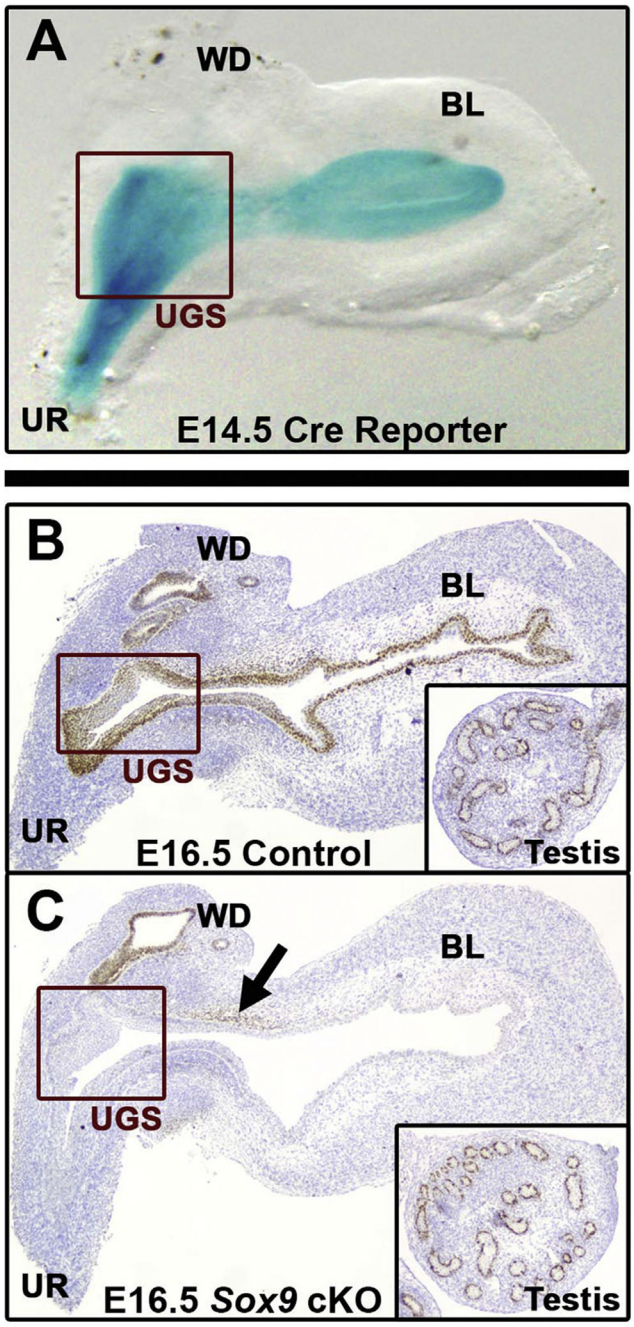

Fig. 2.

Conditional knockout of *Sox9* in UGE and confirmation of loss of SOX9 expression in lower urinary tract epithelium. Conditional knockout of *Sox9* (cKO *Sox9*) in the UGE was mediated by *Shh* driven cre recombinase expression. (A) Lower urinary tract of an E14.5 cre Reporter male fetus stained with Bluo-gal. Blue staining indirectly shows cre recombinase expression restricted to epithelium of the bladder, UGS, and urethra (20x). (B and C) IHC showing SOX9 expression (brown) in sagittal sections of the lower urogenital tract and testis (inset, bottom right) from a representative control (B) and *Sox9* cKO (C) fetus at E16.5 (40x

magnification; nuclei counterstained blue with hematoxylin). The UGS is identified by a red, rectangular box. In the control fetus (B), SOX9 expression is seen throughout epithelium of the lower urogenital tract. In the *Sox9* cKO fetus (C) SOX 9 expression was completely absent from epithelium of the bladder (BL), UGS, and urethra (UR) prior to prostatic budding. Specificity of the conditional *Sox9* knockout is demonstrated by normal SOX9 expression in Wolffian ducts (WD), mesenchymal patch (arrow), and Sertoli cells of the testis in *Sox9* cKO fetuses. All images are representative of n = 3 litter-independent male fetuses.

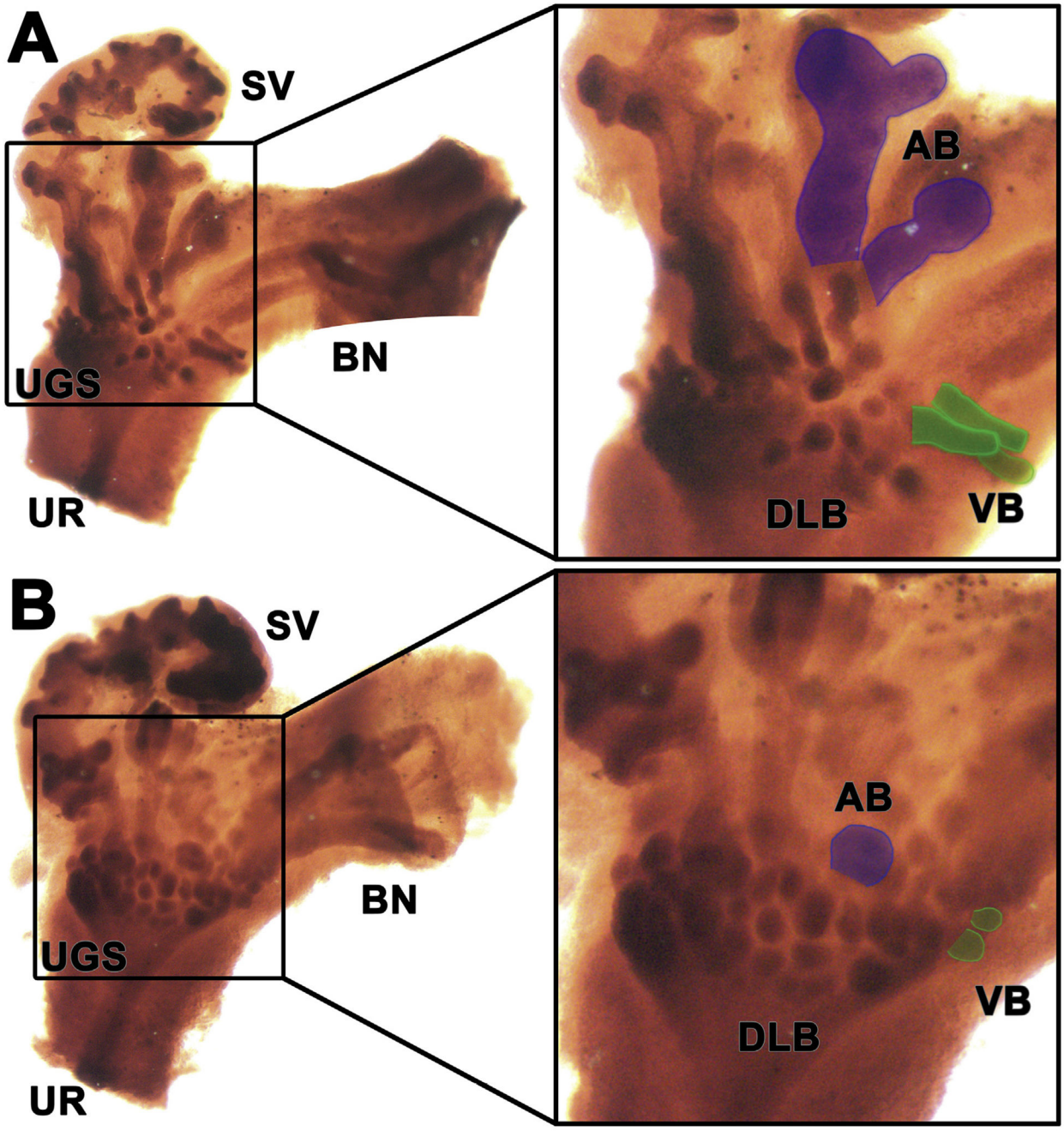

Fig. 3. Conditional knockout of *Sox9* in the male mouse UGE prevents prostatic bud elongation.

WM IHC for cadherin-1 (CDH1) stained epithelium in control male UGS (A) and *Sox9* cKO male UGS (B). *Sox9* is knocked out specifically in the UGE, before prostatic budding initiation begins. The representative control UGS (A) and *Sox9* cKO UGS (B) were harvested at P0.5 from mouse neonates from the same litter. For each UGS, the right panel is an enlargement of the UGS (boxed area) in the left panel (20x). All bud types in the *Sox9* cKO UGS failed to elongate. From this view (right panels), failed elongation of buds in the *Sox9* cKO UGS (B) is most easily observed for anterior buds (AB, pseudocolored blue) and

ventral buds (VB, pseudocolored green). Abbreviations: bladder and bladder neck (BL), seminal vesicle (SV), urethra (UR), dorsolateral buds (DLB) and urogenital sinus (UGS).

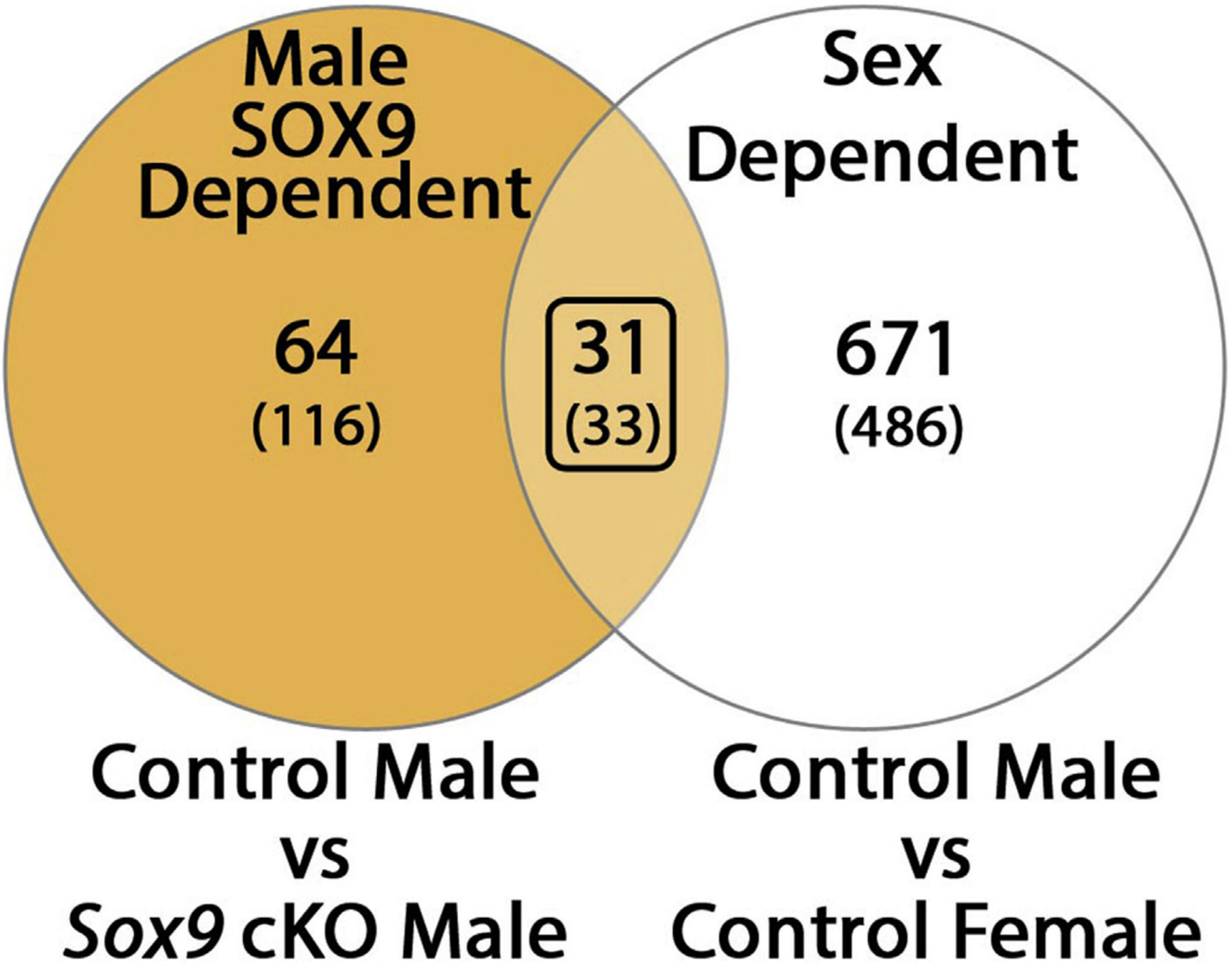

Fig. 4. Expression of 31 genes in male mouse UGE is both *Sox9*-dependent and sex-dependent.
Union (light tan) of the Venn diagram shows 31 genes in the male UGE at E16.75 that have *Sox9*-dependent expression (tan, control male *vs Sox9* cKO male) in common with sex-dependent expression (white, control male *vs* control female). Also 18 of these 31 genes are candidates for promoting bud formation and 3 are candidates for inhibiting bud formation (Table 3). Results for males are based on n = 6 litter independent, male UGEs for both control and *Sox9* cKO groups, respectively, and results for females are based on n = 5 litter independent, female UGEs for both control and *Sox9* cKO groups.

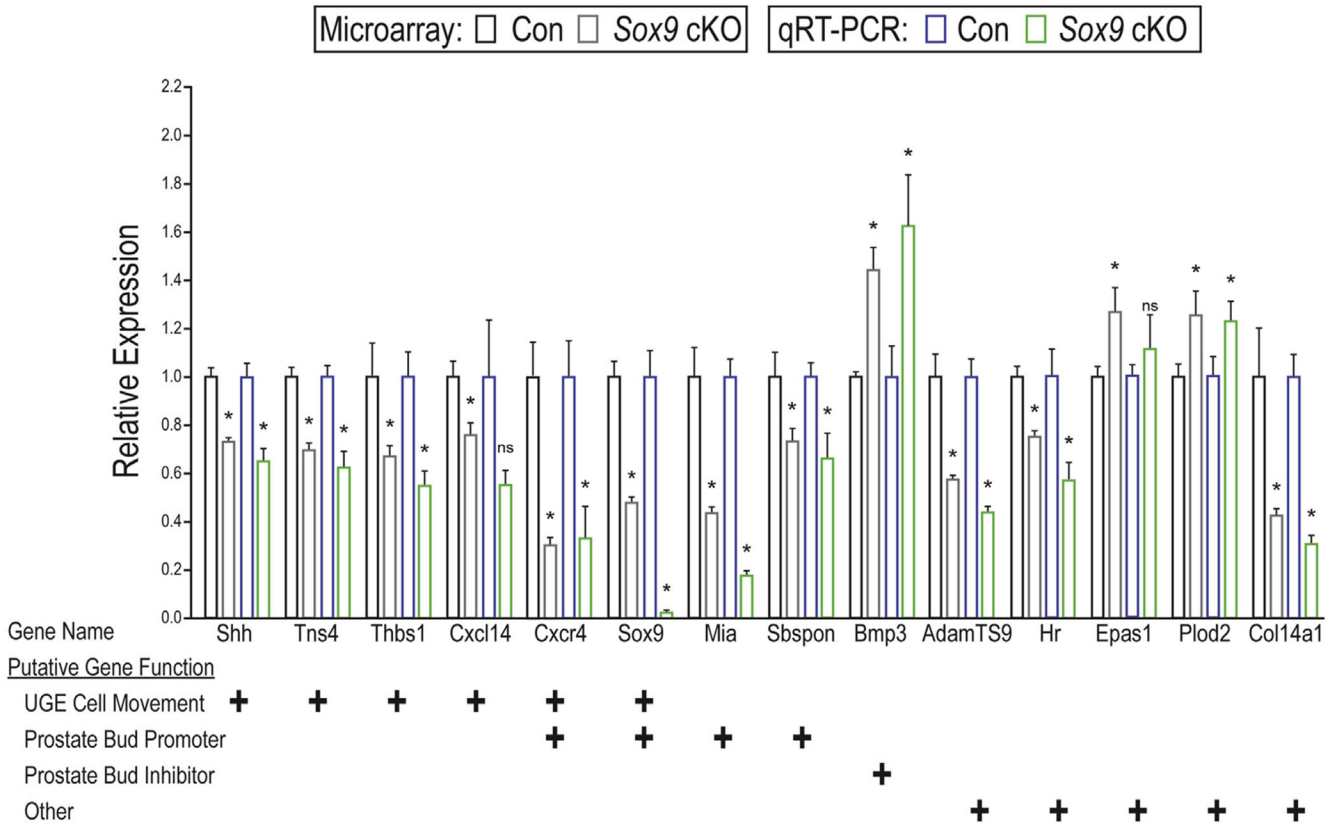

Fig. 5.

Confirmation of *Sox9*-dependent genes in male mouse UGE by PCR and microarray. Comparison of microarray analysis to qRT-PCR in determining relative expression of *Sox9*-dependent transcripts in the UGE of control (Con) *vs Sox9* cKO male mouse fetuses at E16.75. Genes selected for this comparison were initially identified by microarray analysis as being *Sox9*-dependent by comparing their relative transcript abundance between control male *vs Sox9* cKO UGEs at E16.75. Some of these *Sox9*-dependent genes were then discovered by gene ontology analysis to function in cell migration or other functions while other *Sox9*-dependent genes in the male were identified as putative prostatic bud promoters and inhibitors. *Sox9*-dependent genes, within these functional groupings, were selected for confirmation of differential expression by qRT-PCR. UGEs were assessed by microarray (n = 6, both groups) and qRT-PCR (n = 4, both groups). UGEs analyzed by qRT-PCR were separate and distinct from those analyzed by microarray. The expression of these transcripts in control samples, determined by microarray from the bi-weight average signal, has been set to 1.0, while the expression in *Sox9* cKO samples is shown as the fold-change of *Sox9* cKO signal, to control signal. For each transcript analyzed with qRT-PCR, the average expression relative to *Actb1* ($2^{-\Delta Ct}$) in control UGEs have been set to 1.0. Expression of these transcripts relative to *Actb1* in *Sox9* cKO samples is shown as the fold-change of the relative expression seen in controls ($2^{-\Delta\Delta Ct}$). For both methods error bars represent SEM. Asterisks indicate a significant difference between control and *Sox9* cKO ($p \leq 0.05$) when the same method of gene expression analysis is used; *ns* indicates no significant difference ($p > 0.05$). Abbreviations: conditional knockout (cKO), urogenital epithelium (UGE),

standard error of the mean (SEM) and quantitative reverse transcriptase-polymerase chain reaction (qRT-PCR).

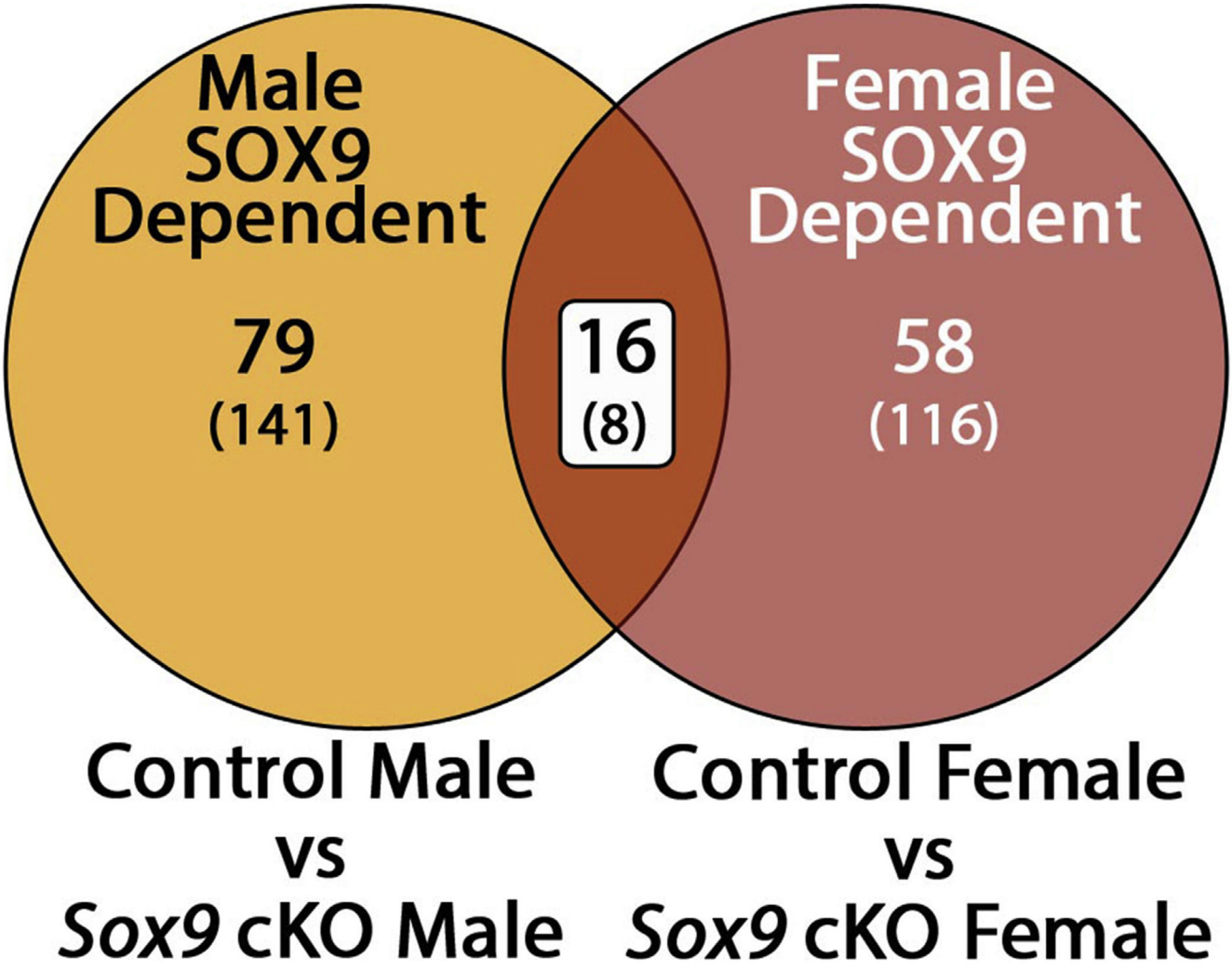

Fig. 6. Only a few *Sox9*-dependent genes in mouse UGE are "common" to both sexes.

Union (dark tan) of the Venn diagram shows that 16 genes exhibit *Sox9*-dependent expression in both male and female UGEs at E16.75. The number of *Sox9*-dependent genes that are significantly upregulated and downregulated (± 1.3 fold, $p \leq 0.05$) are given for male UGEs (tan) and female UGEs (red) based on a comparison of gene expression (control *vs* *Sox9* cKO) within each sex. For each sex, the number of differentially regulated, annotated transcripts is shown at the top, and unannotated transcripts in parentheses at the bottom. Names of the 16 *Sox9*-dependent genes, common to both sexes (union, dark tan), are given in Table 4. Results for males are based on n = 6 litter independent, male UGEs for both control and *Sox9* cKO groups, respectively. Findings for females are based on n = 5 litter independent, female UGEs for both control and *Sox9* cKO groups.

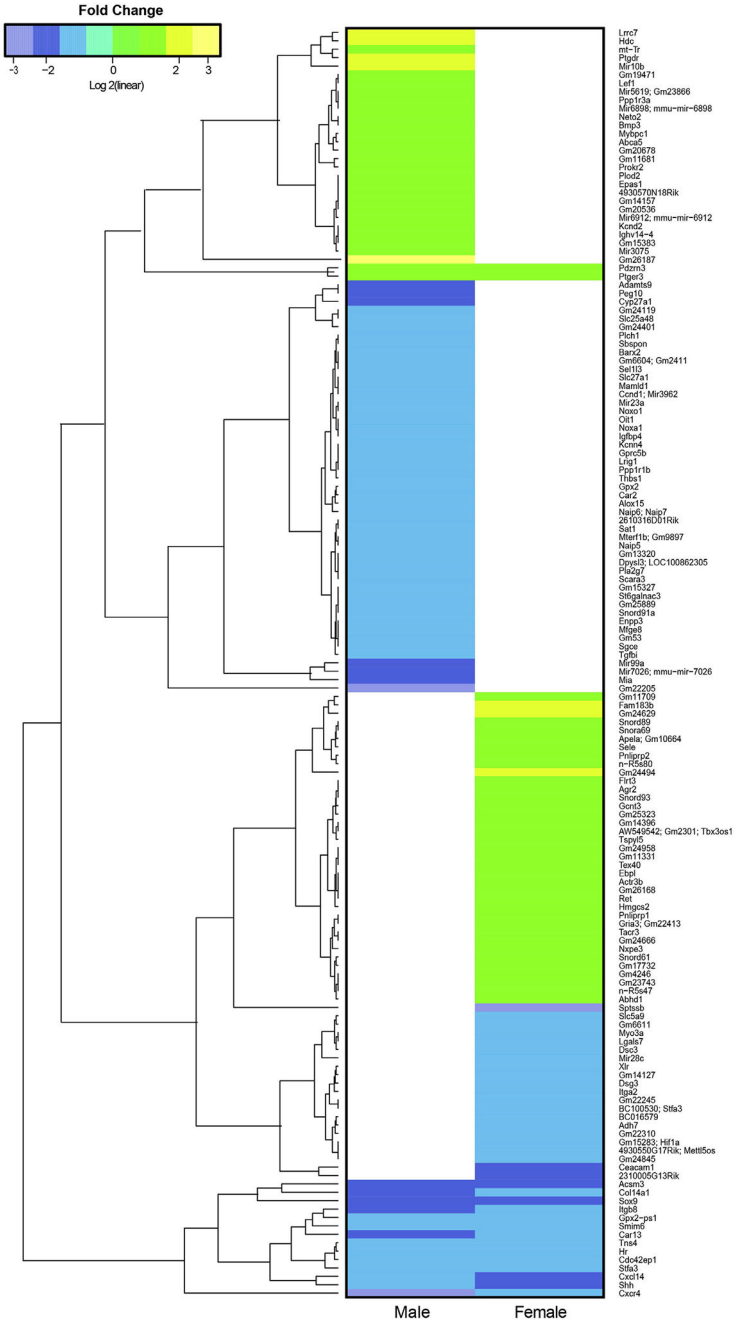

Fig. 7. Sex-dependent differences characterize the *Sox9* deficient, UGE transcriptome of the mouse fetus.

Heatmap of 151 differentially expressed, *Sox9*-dependent genes are shown for the “Male” and “Female” mouse UGE at E16.75 (Supplementary Table 8). Fold change in expression of individual genes in the “Male” [*Sox9* cKO male *vs* control male] and “Female” [*Sox9* cKO female *vs* control female] UGE is depicted in the heatmap as yellow (upregulated) and blue (down-regulated). Of these 151 genes, 16 (11%) were significantly different from control in both sexes (regulated in common); 58 (38%) were significantly different from control only in the “Female” and 77 (51%) were different only in the “Male”. Results for males are based

on n = 6 litter independent, male UGEs for both control and *Sox9* cKO groups, respectively. Findings for females are based on n = 5 litter independent, female UGEs for both control and *Sox9* cKO groups.

Gene Expr Patterns. Author manuscript; available in PMC 2020 December 01.

Table 1

Study design.

Mating Scheme	**Offspring UGS**[a]			
Dam x Sire	**Genotype 1**	**Genotype 2**	**Group**	**Experimental Use**[b] **(day)**
ROSA26 Reporter x *Shh*$^{cre/+}$	ROSA26-βgal +	*Shh*$^{cre/+}$	Cre Reporter	β-Galactosidase Staining (E14.5)
Shh$^{+/+}$; *Sox9*$^{fl/fl}$ x *Shh*$^{cre/+}$; *Sox9*$^{fl/+}$	***Shh***$^{+/+}$	***Sox9***$^{fl/+}$	**Control**	**IHC (E16.5) WM IHC (E18.5-P0.5) Array (E16.75) qRT-PCR (E16.75)**
	Shh$^{+/+}$	*Sox9*$^{fl/fl}$	Control	WM IHC (E18.5-P0.5)
	Shh$^{cre/+}$	*Sox9*$^{fl/+}$	*Sox9* Het	WM IHC (E18.5-P0.5)
	Shh$^{cre/+}$	***Sox9***$^{fl/fl}$	***Sox9* cKO**	**IHC (E16.5) WM IHC (E18.5-P0.5) Array (E16.75) qRT-PCR (E16.75)**

[a] UGSs collected from male fetuses at E14.5, 16.5, 16.75 or 18.5-P0.5 and from female fetuses at E16.75 were used in the present study.

[b] Abbreviations: immunohistochemistry (IHC), whole mount immunohistochemistry (WM IHC), microarray (Array), and quantitative reverse transcription polymerase chain reaction (qRT-PCR). Embryonic day (E) or postnatal day (P) of UGS tissue harvest.

Table 2

Gene ontology analysis of male *Sox9* cKO UGE transcriptome predicts decreased UGE cell migration.

GO Terms	Z Score[a]	# Genes	Downregulated Genes	Upregulated Genes
Cell Movement	− 2.1	23	ALOX15, BARX2, CCND1, CDC42EP1, CXCL14, CXCR4, DPYSL3, IGFBP4, ITGB8, KCNN4, LRIG1, mir-23a, NOXA1, PLA2G7, SHH, SOX9, TGFBI, THBS1, TNS4	HDC, LEF1, mir-lOb, PTGDR
Migration of Cells	− 2.4	22	ALOX15, BARX2, CCND1, CDC42EP1, CXCL14, CXCR4, DPYSL3, IGFBP4, ITGB8, NOXA1, PLA2G7, SHH, SOX9, TGFBI, THBS1, KCNN4, mir23a, TNS4	HDC, PTGDR, LEF1, mir-10b
Chemotaxis of Cells	− 2.6	8	CCND1, CXCL14, CXCR4, KCNN4, PLA2G7, THBS1	LEF1, PTGDR
Cell movement of Phagocytes	− 2.0	7	CCND1, CXCL14, CXCR4, PLA2G7, THBS1	mir-10b, PTGDR
Chemotaxis of Phagocytes	− 2.4	6	CCND1, CXCL14, CXCR4, PLA2G7, THBS1	PTGDR
Chemotaxis of Myeloid cells	− 2.2	5	CCND1, CXCL14, CXCR4, PLA2G7, THBS1	
Chemotaxis Antigen Presenting Cells	− 2.2	5	CCND1, CXCL14, CXCR4, THBS1	PTGDR
Adhesion of Tumor Cell Lines	− 2.1	5	ALOX15, CCND1, CXCR4, THBS1	LEF1
Glucose Metabolism Disorder	− 2.2	21	ADAMTS9, ALOX15, CAR13, CAR2, CCND1, COL14A1, CXCL14, CXCR4, DPYSL3, LRIG1, mir-23, Naip7, SLC27A1, TGFBI, HBS1	FLRT3, HIF1A, PNLIPRP1, PTGER3, RET, TACR3
Fibrogenesis	− 2.2	6	ALOX15, CCND1, DPYSL3, TGFBI, TNS4	EPAS1

[a]Z score ≤ − 2.0 is significantly decreased.

Table 3

Putative regulators of bud development.

ARRAY EXPERIMENTAL DESIGN		*sox9* CKO MALE	vs	CONTROL MALE	CONTROL MALE	vs	CONTROL FEMALE
(Prostate Bud Development)		(Stunted)		(Normal)	(Normal)		(None)
MGI[a] Gene ID	Gene Symbol	Male SOX9 Dependent Fold Change			Sex Dependent Fold Change		
Putative Promoters							
99538	***Acsm3***	*− 1.9*			**1.5**		
87997	***Alox15***	*−1.5*			**1.5**		
109563	***Cxcr4***	*− 3.1*			**2.8**		
88594	***Cyp27a1***	*−1.7*			**1.9**		
5454178	***Gm24401***	*−1.6*			**1.4**		
5455666	***Gm25889***	*− 1.4*			**1.3**		
109615	***Mia***	*− 2.2*			**1.8**		
2676897	***Mir23a***	*− 1.4*			**1.4**		
2676912	***Mir99a***	*−2.0*			**1.7**		
1298220	***Naip5***	*− 1.3*			**1.7**		
1298222; 1858256	***Naip6; Naip7***	− 1.5			**2.1**		
2449980	***Noxal***	*− 1.4*			**1.5**		
1201784	***Oit1***	*− 1.4*			**1.4**		
94860	***Ppp1r1b***	*− 1.4*			**1.6**		
2684952	***Sbspon***	*− 1.4*			**3.7**		
2145373	***Slc25a48***	*− 1.6*			**1.5**		
98371	***Sox9***	*− 2.0*			**1.4**		
1341828	***St6galnac3***	*− 1.4*			**1.3**		
Putative Inhibitors							
88179	***Bmp3***	**1.5**			*− 1.3*		
5453643	***Mir5619***	**1.4**			*−1.4*		
102476	***mt-Tr***	**1.6**			*− 1.8*		

[a]Mouse Genome Informatics (www.informatics.jax.org).

Table 4

SOX9 dependent genes differentially expressed, in common, in male and female UGEs at E16.75.

Groups Compared:		***Sox9* cKO vs Control**	
MGI[a] Gene ID	**Gene Symbol**	**Male Fold Change**	**Female Fold Change**
98371	*Sox9*	*−2.0*	−2.1
Downregulated in	***Sox9* cKO[b]**		
99538	***Ascm3***	*−1.9*	−1.8
1931322	***Car13***	*−1.7*	−1.4
1929763	***Cdc42ep1***	*−1.3*	−1.3
1341272	***Col14a1***	*−2.1*	−1.6
1888514	***Cxcl144***	*−1.3*	−1.6
109563	***Cxcr4***	*−3.1*	−1.6
106627	***Gpx2-ps1***	*−1.5*	−1.3
96223	***Hr***	*−1.4*	−1.3
1338035	***Itgb8***	*−1.6*	−1.3
98297	***Shh***	*−1.4*	−1.7
1915778	***Smim6***	*−1.5*	−1.4
106196	***Stfa3***	*−1.4*	−1.4
2144377	***Tns4***	*−1.4*	−1.3
Upregulated in *Sox9* cKO[c]			
1933157	***Pdzrn3***	**1.3**	1.3
97795	***Ptger3***	**1.3**	1.4

[a]Mouse Genome Informatics (www.informatics.jax.org).

Key resources Table

Reagent or resource	Source	Identifier
Antibodies		
Rabbit Monoclonal Anti-SOX9	Abcam	Cat# ab185230, RRID:AB_2715497
Rabbit Monoclonal Anti-CDH1	Cell Signaling	Cat#: 3195, RRID:AB_2291471
Biotinylated Goat Anti-rabbit IgG	Vector Labs	Cat#: BA-1000, RRID:AB_2313606
Horse Anti-rabbit IgG, ImmPRESS VR Reagent	Vector Labs	Cat#: MP-6401, RRID:AB_2336529
Bacterial and Virus Strains		
None		
Biological Samples		
Goat Serum	Millipore-Sigma	Cat#: G9023
Bovine Serum Albumin	Millipore-Sigma	Cat#: 29-102-5 GM
Trypsin	Difco	Cat#: 215240
Collagenase	Millipore-Sigma	Cat#: C9891
Chemicals, Peptides, and Recombinant Proteins		
Bluo-gal	Gold Biotechnology	Cat#: B-673-250
Critical Commercial Assays		
Agilent RNA 6000 Pico	Agilent Technologies	Cat#: 5067-1513
GeneChip Mouse Gene 1.0 ST Array	ThermoFisher Scientific	Cat#: 901171
Deposited Data		
RNA Microarray Data	NCBI GEO Database	GSE113011; reviewer token mhizgciwxxcxbyl
Experimental Models: Cell Lines		
None		
Experimental Models: Organisms/Strains		
Mouse: C57BL/6J	Jackson Laboratory	Stock#:000664, RRID: IMSR_JAX: 000664
Mouse: *B6.129S4-Gt(ROSA)26*^{sortm1Sor}/J	Jackson Laboratory	Stock# 003474, RRID: IMSR_J AX: 003474
Mouse: B6. CgShh$^{tm1(EGFP/cre)Cjt}$/J	Jackson Laboratory	Stock#005622; RRID: IMSR_J AX: 005622
Mouse: B6.129S7-Sox9^{tm2Crm}/J	Jackson Laboratory	Stock#: 013106, RRID:IMSR_JAX:013106
Oligonucleotides		
See Supplemental Table 11 for TaqMan Probe ID	ThermoFisher Scientific	
Recombinant DNA		
None		
Software and Algorithms		
Transcriptome Analysis Console	ThermoFisher Scientific	
Ingenuity Pathway Analysis	QIAGEN	
R	www.r-project.org	
Sequence Detection System v 2.-4.	ThermoFisher Scientific	
Other		
ImmPACT DAB Staining Kit	Vector Labs	Cat#: SK-4105
Hematoxylin QS	Vector Labs	Cat#: H-3404
Peroxidase-conjugated Streptavidin	Vector Labs	Cat#: PK-6100
RNeasy Mini Kit	QIAGEN	Cat#: 74104

Reagent or resource	Source	Identifier
GeneChip WT Pico Reagent Kit	ThermoFisher Scientific	Cat#: 902623
High Capacity cDNA Reverse Transcription Kit	ThermoFisher Scientific	Cat#: 4368814
TaqMan Preamp Mastermix Kit	ThermoFisher Scientific	Cat#: 4384267